NASA GEOS Composition Forecast Modeling System GEOS-CF v1.0: Stratospheric composition

K. Emma Knowland[1], Christoph A. Keller[1], Pamela A Wales[2], Krzysztof Wargan[3], Lawrence Coy[4], Matthew S Johnson[5], Junhua Liu[1], Robert A Lucchesi[6], Sebastian David Eastham[7], Eric L. Fleming[8], Qing Liang[9], Thierry Leblanc[10], Nathaniel J Livesey[10], Kaley A. Walker[11], Lesley E. Ott[12], and Steven Pawson[12]

[1]Universities Space Research Association
[2]University of Maryland, College Park
[3]Science Systems and Applications, Inc.
[4]SSAI
[5]NASA Ames Research Center
[6]Science Systems and Applications, Inc
[7]Massachusetts Institute of Technology
[8]NASA/Goddard Space Flight Center, Science Systems and Applications, Inc.
[9]NASA GSFC
[10]Jet Propulsion Laboratory
[11]University of Toronto
[12]NASA Goddard Space Flight Center

November 22, 2022

Abstract

The NASA Goddard Earth Observing System (GEOS) Composition Forecast (GEOS-CF) provides recent estimates and five-day forecasts of atmospheric composition to the public in near-real time. To do this, the GEOS Earth system model is coupled with the GEOS-Chem tropospheric-stratospheric unified chemistry extension (UCX) to represent composition from the surface to the top of the GEOS atmosphere (0.01 hPa). The GEOS-CF system is described, including updates made to the GEOS-Chem UCX mechanism within GEOS-CF for improved representation of stratospheric chemistry. Comparisons are made against balloon, lidar and satellite observations for stratospheric composition, including measurements of ozone (O_3) and important nitrogen and chlorine species related to stratospheric O_3 recovery. The GEOS-CF nudges the stratospheric O_3 towards the GEOS Forward Processing (GEOS FP) assimilated O3 product; as a result the stratospheric O_3 in the GEOS-CF historical estimate agrees well with observations. During abnormal dynamical and chemical environments such as the 2020 polar vortexes, the GEOS-CF O_3 forecasts are more realistic than GEOS FP O_3 forecasts because of the inclusion of the complex GEOS-Chem UCX chemistry. Overall, the spatial pattern of the GEOS-CF simulated concentrations of stratospheric composition agrees well with satellite observations. However, there are notable biases – such as low NO_x and HNO_3 in the polar regions and generally low HCl throughout the stratosphere – and future improvements to the chemistry mechanism and emissions are discussed. GEOS-CF is a new tool for the research community and instrument teams observing trace gases in the stratosphere and troposphere, providing near-real-time three-dimensional gridded information on atmospheric composition.

NASA GEOS Composition Forecast Modeling System GEOS-CF v1.0: Stratospheric composition

K. E. Knowland[1,2], C. A. Keller[1,2], P. A. Wales[1,2], K. Wargan[2,3], L. Coy[2,3], M. S. Johnson[5], J. Liu[1,4], R. A. Lucchesi[2,3], S. D. Eastham[6,7], E. Fleming[3,4], Q. Liang[4], T. Leblanc[8], N. J. Livesey[9], K. A. Walker[10], L. E. Ott[2], S. Pawson[2]

[1]Universities Space Research Association (USRA)/GESTAR, Columbia, MD, USA
[2]NASA Goddard Space Flight Center (GSFC), Global Modeling and Assimilation Office (GMAO), Greenbelt, MD, USA
[3]Science Systems and Applications (SSAI), Inc., Lanham, MD, USA
[4]Atmospheric Chemistry and Dynamics Laboratory, NASA GSFC, Greenbelt, MD, USA
[5]Earth Science Division, NASA Ames Research Center, Moffett Field, CA, USA
[6]Laboratory for Aviation and the Environment, Department of Aeronautics and Astronautics, Massachusetts Institute of Technology, Cambridge, MA, USA
[7]Joint Program on the Science and Policy of Global Change, Massachusetts Institute of Technology, Cambridge, MA, USA
[8]Jet Propulsion Laboratory, California Institute of Technology, Wrightwood, CA, USA
[9]Jet Propulsion Laboratory, California Institute of Technology, Pasadena, CA, USA
[10]University of Toronto, Department of Physics, Toronto, Canada

Key Points:

- Demonstrate the GEOS-CF system is capable of supporting NASA science missions and applications which observe stratospheric composition
- The GEOS-CF model produces realistic stratospheric ozone forecasts, a new capability during anomalous polar vortex conditions
- Spatial patterns of the GEOS-CF simulated concentrations of stratospheric composition agree well with independent observations

---

Corresponding author: K. Emma Knowland, `k.e.knowland@nasa.gov`

Abstract

The NASA Goddard Earth Observing System (GEOS) Composition Forecast (GEOS-CF) provides recent estimates and five-day forecasts of atmospheric composition to the public in near-real time. To do this, the GEOS Earth system model is coupled with the GEOS-Chem tropospheric-stratospheric unified chemistry extension (UCX) to represent composition from the surface to the top of the GEOS atmosphere (0.01 hPa). The GEOS-CF system is described, including updates made to the GEOS-Chem UCX mechanism within GEOS-CF for improved representation of stratospheric chemistry. Comparisons are made against balloon, lidar and satellite observations for stratospheric composition, including measurements of ozone (O_3) and important nitrogen and chlorine species related to stratospheric O_3 recovery. The GEOS-CF nudges the stratospheric O_3 towards the GEOS Forward Processing (GEOS FP) assimilated O_3 product; as a result the stratospheric O_3 in the GEOS-CF historical estimate agrees well with observations. During abnormal dynamical and chemical environments such as the 2020 polar vortexes, the GEOS-CF O_3 forecasts are more realistic than GEOS FP O_3 forecasts because of the inclusion of the complex GEOS-Chem UCX stratospheric chemistry. Overall, the spatial patterns of the GEOS-CF simulated concentrations of stratospheric composition agree well with satellite observations. However, there are notable biases – such as low NO_x and HNO_3 in the polar regions and generally low HCl throughout the stratosphere – and future improvements to the chemistry mechanism and emissions are discussed. GEOS-CF is a new tool for the research community and instrument teams observing trace gases in the stratosphere and troposphere, providing near-real-time three-dimensional gridded information on atmospheric composition.

Plain Language Summary

In the stratosphere, the ozone layer protects life on Earth from harmful ultraviolet, "UV", radiation. Chemical loss of this protective ozone occurs each year over Antarctica and occasionally over the Arctic during spring when air over these regions are cut-off from the rest of the stratosphere because of the strong winds blowing circularly around the pole. For accurate forecasting of the ozone layer and UV, it is critical to have both meteorology and chemistry accurately represented in forecast models. NASA's Goddard Earth Observing System composition forecast, "GEOS-CF", produces global five-day forecasts of weather and atmospheric trace gases that are important for tracking the chemical interactions in the full atmosphere. Additionally, weather systems can bring down stratospheric ozone towards the Earth's surface where ozone is a regulated air pollutant. GEOS-CF can differentiate between ozone enhancements at the Earth's surface that result from pollution and from stratospheric transport, improving the forecasts of stratospheric-influenced ozone exceedance events. This study describes the GEOS-CF model system and evaluates the modeled representation of stratospheric trace gases. GEOS-CF products are used to support NASA ground and satellite-based instrument teams as well as field and aircraft campaigns that measure trace gases throughout the atmosphere.

1 Introduction

NASA's Global Modeling and Assimilation Office (GMAO) provides a suite of Goddard Earth Observing System (GEOS) Earth system model (ESM) products to the public in near-real time (analyses and forecasts) and with a month to two month latency (reanalysis) (`https://gmao.gsfc.nasa.gov/GMAO_products/`). These products assimilate weather, aerosol and stratospheric ozone (O_3) observations and are used to support NASA field missions and assess the impacts of NASA observations on environmental prediction. To further support the research community and NASA missions with atmospheric composition simulations, the state-of-the-science GEOS-Chem chemistry transport model (CTM; Bey et al., 2001) is integrated into the GEOS ESM (Keller et al., 2014; Long et al., 2015; Hu et al., 2018). Owing to the complexity of the chemistry, with 250 reactions and 725 chemical species in GEOS-Chem version 12.0.1, this coupled configuration is run once daily and provides detailed composition forecasts ("GEOS-CF") of the three-dimensional (3D) state of the atmosphere on the same spatial (0.25^o) resolution as the meteorology (Keller et al., 2021). This current study evaluating the GEOS-CF stratospheric composition (up to 1 hPa) is a companion paper to the GEOS-CF description paper by Keller et al. (2021) which evaluated tropospheric composition and surface air quality forecast skill against independent observations.

GEOS-Chem was initially designed as a global 3D CTM driven by assimilated GEOS meteorological fields (Bey et al., 2001). It has an extensive community of developers and users worldwide (`http://acmg.seas.harvard.edu/geos/`). As the tropospheric chemistry became increasingly more sophisticated in GEOS-Chem, the stratospheric chemical boundary condition became a limiting factor for stratosphere-troposphere coupling analysis (Eastham et al., 2014). Over a similar time frame, the NASA Global Modeling Initiative (GMI) chemistry mechanism was developed at NASA Goddard Space Flight Center and is maintained to be state-of-the-science for stratospheric chemistry modeling to support policy relevant assessments on stratospheric composition and O_3 recovery (e.g., Douglass et al., 1999, 2004; Kinnison et al., 2001; Rotman et al., 2001; Duncan et al., 2007; Bucsela et al., 2013; Nielsen et al., 2017; Strahan & Douglass, 2018). Using a version of the NASA GMI stratospheric chemistry mechanism, updated with the Jet Propulsion Laboratory (JPL)'s stratospheric recommendations for kinetic and photochemical data (JPL Publication 10-06; Sander et al., 2011), Eastham et al. (2014) extended GEOS-Chem to have the capability to run with a unified tropospheric and stratospheric chemistry mechanism, "UCX". The GEOS-Chem model has continued to evolve since the version 9 evaluated in Eastham et al. (2014), with updates which could impact stratospheric composition such as the treatment of halogen species (Schmidt et al., 2016; Sherwen, Evans, et al., 2016; Sherwen, Schmidt, et al., 2016; Chen et al., 2017). This present study benchmarks the stratospheric composition using a more recent version of GEOS-Chem (version 12.0.1) run in an online high-resolution global GEOS simulation (GEOS-CF) to assess the readiness of GEOS-CF output to support the research community and to prioritize needed improvements.

GEOS-CF is designed to support a broad range of near-real-time NASA applications focused on atmospheric composition, including satellite and ground-based instrument retrievals of trace gases, field and airborne campaigns, and stratosphere-troposphere exchange. For such research activities, it is essential GEOS-CF has a realistic representation of stratospheric composition and chemistry (Nielsen et al., 2017). Ozone is an important trace gas in the stratosphere where the total O_3 column acts to shield the Earth's surface from harmful ultra-violet (UV) radiation, while at the surface it is harmful to human health and vegetation (Schlink et al., 2006; Krzyzanowski & Cohen, 2008). Since the total column O_3 (TCO) varies from day-to-day depending on stratospheric conditions, forecasting TCO is an important input for accurate surface UV forecasts (Turner et al., 2017). The discovery of the Antarctic "Ozone hole" nearly 40 years ago by ground-based, sonde and satellite measurements (e.g., Farman et al., 1985; Solomon et al., 1986; Stolarski et al., 1986) indicated decreases in the ozone layer were greater than the 1 % per decade that early models were predicting (Bhartia & McPeters, 2018). Tracking the recovery of the Antarctic ozone hole requires the sustained combination of high quality observations and models.

The GMAO has a mature data assimilation system (DAS) within GEOS to provide a realistic global 3D stratospheric O_3 product for the "satellite era" (since 1980) (Wargan et al., 2015, 2017; Wargan, Kramarova, et al., 2020; Wargan, Weir, et al., 2020) which can be used in analysis of stratospheric O_3 trends (Wargan et al., 2018). For five to ten day TCO forecasting, GMAO's state-of-the-science numerical weather prediction GEOS Forward Processing (GEOS FP; Lucchesi, 2018) system assimilates near-real time

O_3 observations. However, the GEOS FP forecasts rely on simple parameterized chemistry based on fixed, pre-calculated, monthly, latitude/altitude production and loss values as described in Nielsen et al. (2017). In contrast, for GEOS-CF, the combination of the sophisticated GEOS-Chem chemistry within a GEOS forecasting system allows for improved forecasting of TCO when far from climatological values and, for the first time, provides near-real time 3D estimates of chemical species that are critical for understanding stratospheric O_3 recovery and loss, such as nitrogen oxides (NO_x) and hydrogen chloride (HCl).

The paper follows with an overview of the GEOS-CF system (Section 2), followed by the description of the independent observations – those which do not constrain the GEOS-CF constituent concentrations – that are used for validation (Section 3). Additional updates to the UCX code for the GEOS-CF system are outlined in Section 4. The evaluation against ozonesondes, lidar and satellite observations is presented in Section 5, with case studies of forecast skill in Section 5.3. Final summary and future developments are discussed in Section 6.

2 GEOS Composition Forecast (GEOS-CF) model description

The NASA GEOS-CF system (Keller et al., 2021) is a near-real time global 3D coupled chemistry and meteorology modeling system with the offline GEOS-Chem CTM code fully integrated as a chemistry module in the GEOS ESM (Long et al., 2015; Hu et al., 2018). The GEOS-Chem chemistry components are therefore the same in GEOS-CF as in the offline CTM except the dynamics and turbulence schemes use the online GEOS ESM meteorology instead of the offline transport scheme within the CTM. Briefly, the GEOS-CF configuration has the GEOS atmospheric general circulation model (AGCM; Molod et al., 2015) one-way coupled to the GEOS-Chem chemistry module, run on a cube-sphere horizontal grid at c360 resolution and on 72 GEOS hybrid-eta model layers from the surface to 0.01 hPa, with output at the global resolution of 0.25^o latitude x 0.25^o longitude (GEOS-CF version 01, "v01", Keller et al., 2021).

Since the GEOS-CF configuration is computationally expensive due to the complexity of the chemistry, it is run once per day and as a separate system from the GEOS FP system. Instead of running a full DAS, GEOS-CF relies on GMAO's meteorological "replay" technique (Orbe et al., 2017), where the AGCM computes the increments for pressure, temperature, wind (U, V), specific humidity, aerosol optical depth and O_3 based on pre-computed analysis fields from a previously run assimilation system. Every day, prior to the launch of the forecast, GEOS-CF replays to the past 24-hours of GEOS FP for Instrument Teams (GEOS FP-IT; Lucchesi, 2015) assimilated meteorology, aerosols and ozone in order to ensure consistent model physics within the AGCM. Unlike GEOS FP, GEOS FP-IT is a static model system, designed to have minimal updates to the system in order to support near-real time retrievals by satellite instrument teams. For similar reasons, a "frozen" model was preferred as the driving meteorology for GEOS-CF v01. It is important to note that in GEOS-CF the GEOS-Chem aerosols and ozone are run passively, therefore do not directly impact the dynamics nor are the increments applied to the GEOS-Chem aerosols and ozone.

In the GEOS-CF v01, there is no direct data assimilation of chemical species; however, near-real time satellite observations of (1) fire radiative power and (2) stratospheric O_3 are incorporated into GEOS-CF during the replay segments. Specifically: (1) the Quick Fire Emissions Dataset (QFED; Darmenov & da Silva, 2015) informs the model of recent fires, which is then persisted forward for each five-day forecast; and (2) the GEOS-CF stratospheric O_3 (pressures less than approximately 56 hPa) is nudged towards the GEOS FP assimilated O_3 3-hourly average product. The GEOS FP ozone observing system includes the limb-sounding profiles from the near-real time Microwave Limb Sounder (MLS; Waters et al., 2006) product, column-based measurements from Ozone Monitoring Instrument (OMI; Levelt et al., 2006, 2018) and, after March 2019, the O_3 observing system was updated to include TCO from Ozone Mapping and Profiler Suite Nadir Mapper (OMPS-NM; Bak et al., 2017) instrument aboard Suomi National Polar-Orbiting Partnership (SNPP). The nudging method is intended to keep stratospheric O_3 in line with observations on a seasonal time scale while still allowing GEOS-Chem to simulate complex chemical interactions in the troposphere and stratosphere. The nudging technique in GEOS-CF v01 is as follows: from the top of the atmosphere (GEOS level 1) down to lower stratosphere (GEOS level 33, approximately 40 hPa), the O_3 is nudged 20 % toward the GEOS FP O_3 during every time step (5 minutes). There is not a hard cut off in the nudging, but instead from levels 33 to 35 (approximately 56 hPa, well above the tropopause), there is a smooth transition, and then from GEOS level 35 to 72 (model's lowest layer), the O_3 is not constrained.

This replay set-up provides the best initial conditions for the five-day forecast initialized at 12 UTC (See Figure 1 of Keller et al., 2021). Since the end of each replay segment is used to start the next day's replay simulation, these 24-hour segments can be considered as a continuous model best estimate of the 3D composition of the atmosphere, starting 1 January 2018 for GEOS-CF v01.

In this study, the replay estimates of stratospheric composition will be the main focus of the evaluation. The GEOS-CF five-day forecasts remain available to the public for a two-week period, and are archived at the NASA Center for Climate Simulation (NCCS) for posterity. In Section 5.3, the forecast skill for TCO will be presented for two case study periods and an example of forecasting the impact of stratospheric O_3 on tropospheric composition is reported. Full details of the GEOS-CF model set-up, including emission data sets, and available model output can be found in Keller et al. (2021) and Knowland et al. (2020), respectively.

3 Data

In this section, the remote-sensing and balloon-based observation datasets used for evaluation of the GEOS-CF stratospheric constituents for the year 2020 are described (Table 1). Several hundred chemical species are included in GEOS-Chem, but most of them do not have observations available on a global scale. This manuscript focuses on the satellite observations and the global distribution of ozonesondes that can be used to make general conclusions about the global state of the stratospheric composition in GEOS-CF. Comparisons against regional networks such as the Pandora network or the Tropospheric Ozone Lidar Network (TOLNet) are active areas of research (e.g., Dacic et al., 2020; Robinson et al., 2020; Johnson et al., 2021; Gronoff et al., 2021) as demonstrated with a case study using TOLNet vertically-resolved O_3 measurements (Section 5.3.3).

3.1 Satellite

In addition to limb-sounding O_3 profiles, MLS observes other constituents to high degrees of accuracy which are useful for monitoring O_3 depleting substances (ODS; e.g., halogen bromine (Br) and chlorine (Cl) species) and atmospheric circulation (nitrous oxide (N_2O)). In this study, MLS level 2, version 5 (Livesey et al., 2020) profiles of O_3, water vapor (H_2O), hydrogen chloride (HCl), chlorine monoxide (ClO), nitric acid (HNO_3), and N_2O for 2020 are used (Table 1).

Other independent observations for model evaluation include measurements from two solar occultation instruments: the Stratospheric Aerosol and Gas Experiment (SAGE) III instrument aboard the International Space Station (ISS) and the Atmospheric Chemistry Experiment-Fourier Transform Spectrometer (ACE-FTS) on the Canadian SCISAT satellite. The solar occultation measurements from SAGE III/ISS (June 2017 to present; Cisewski et al., 2014) and ACE-FTS (February 2004 to present; Bernath et al., 2005; Bernath,

Table 1. Overview of Observation Data Sets used for GEOS-CF model validation

Description	**Species**	**Reference**
Satellite		
ACE-FTS v4.1	O_3, H_2O, HCl, HNO_3, N_2O, NO, NO_2, N_2O_5, $ClONO_2$	Boone et al. (2020)
MLS v5	O_3, H_2O, HCl, HNO_3, N_2O	Livesey et al. (2021)
SAGE III/ISS v5.1	O_3	McCormick et al. (2020); H. J. R. Wang et al. (2020)
Ozone Watch	O_3	`https://ozonewatch.gsfc.nasa.gov/`
OMI "TOMS-like" v3 level 3 product	O_3	McPeters et al. (2008); Bhartia (2012)
SBUV Merged Ozone product v8.6	O_3	Frith et al. (2014)
Balloon		
Ozonesondes	O_3	`http://www.woudc.org`, `ftp://aftp.cmdl.noaa.gov/data/ozwv/ozonesonde/`
Ground-based		
TOLNet Lidar	O_3	`https://www-air.larc.nasa.gov/missions/TOLNet`

2017) provide high vertical resolution profiles of O_3, H_2O and other species but there are far fewer observations per day (15 to 30) compared to MLS profiles (3500). SAGE III/ISS has a measurement range from about 70 °S to 70 °N (H. J. R. Wang et al., 2020) while ACE-FTS covers further into the polar regions because of its high orbital inclination (74° compared to 52° for the ISS). The measurements are mainly in the stratosphere, however the retrieved profiles can be extended into the troposphere (generally limited to the cloud top height; Mauldin et al., 1998; Boone et al., 2020) and into the mesosphere (SAGE III/ISS; Mauldin et al., 1998; McCormick & Chu, 2004) and lower thermosphere (ACE-FTS; Boone et al., 2020). Here, SAGE III/ISS version 5.1 and ACE-FTS version 4.1 profiles are used, interpolated to MLS pressure levels and GEOS-CF potential temperature vertical grid.

Along with the satellite level 2 products for the instruments detailed above, publicly available O_3 values from the NASA "Ozone Watch" website (`https://ozonewatch.gsfc.nasa.gov/`) are used for verification of O_3 forecasts. Ozone Watch daily values of the Northern Hemisphere (NH) polar cap total O_3 and the Southern Hemisphere (SH) ozone hole area are historically based on a wide range of satellite observations; since July 2016 it is based on the OMPS-NM. If OMPS-NM data is missing, the Ozone Watch product relies on the near-real time GEOS FP assimilated TCO product. Merged, homogenized satellite products are useful for evaluation of long-term simulations, since biases across multiple instruments are removed relative to a reference dataset; we use version 8.6 of the SBUV Merged Ozone Dataset (Frith et al., 2014) and version 3 of the OMI

"TOMS-like" level 3 gridded product (McPeters et al., 2008; Bhartia, 2012) for this purpose (see Section 4).

3.2 Ozonesonde observations

Ozonesondes provide profile measurements of tropospheric and stratospheric O_3, up to about 30 to 35 km altitude (Thompson et al., 2017; Sterling et al., 2018; Stauffer et al., 2020). Data was selected from 20 of the 24 sites in Keller et al. (2021), distributed globally (Table 2, Figure S1), and accessed through the World Ozone and Ultraviolet Data Center (WOUDC, `http://www.woudc.org`) and from Global Monitoring Laboratory, National Oceanic and Atmospheric Administration (NOAA) network (`ftp://aftp.cmdl.noaa.gov/data/ozwv/ozonesonde/`). Keller et al. (2021) reported on the tropospheric

Table 2. Ozonesonde launch locations, listed from North to South, grouped into 5 latitude bands (see also Figure S1): NH Polar (> 60°), NH Mid-latitudes (30° to 60°), Subtropics/tropics (-30° to 30°), SH Mid-latitudes (-30 to -60°) and SH Polar (< -60°). Number of launches (N) for January to December 2020 are provided.

Station name	**Latitude (°N)**	**Longitude (°E)**	**Launch hour (UTC)**	**N (2020 only)**
NH Polar				
Alert	82.5	-62.3	18 or 23	17
Eureka	80.0	-85.9	11, 18 or 23	65
NH Mid-latitudes				
Legionowo	52.4	21.0	11	41
Valentia	51.9	-10.2	11	30
Uccle	50.8	4.3	11 - 12	144
Praha	50.0	14.4	11	46
Payerne	46.5	6.6	10 - 12	111
Trinidad Head	41.1	-124.2	16 - 21	45
Madrid	40.5	-3.6	10 - 11	54
Boulder	40.0	-105.2	16 - 21	59
Tateno	36.1	140.1	14 - 15	37
Subtropics/tropics				
King's Park	22.3	114.2	5	48
Hilo	19.7	-155.1	18 - 19	50
Pago Pago	-14.3	-170.7	14 - 24	38
Suva	-18.1	178.4	21 - 23	15
SH Mid-latitudes				
Broadmeadows	-37.7	144.9	0 - 3	51
Lauder	-45.0	169.7	19 - 8	54
Macquarie Island	-54.4	158.9	5 or 23	51
SH Polar				
Syowa	-69.0	39.6	2, 8 or 14	46
South Pole	-90.0	169.0	8-11, 20-22	51

portion of the profiles (1000 to 200 hPa) for 2018-2019; this study focuses on stratospheric composition and will evaluate the profiles from 400 to 10 hPa. De Bilt, Pohang, Paramaribo, and Marambio were excluded from this study, as sites were selected using the criteria that each location has at least one observation reported in each month, similar to Steinbrecht et al. (2021). The number of ozonesonde launches in 2020 compared to the number of launches in previous years was reduced at many stations because of COVID-19 restrictions; nonetheless, there were still enough measurements for scientific study at the selected 20 stations (Table 2). At these sites, the frequency of ozonesonde launches is generally once or twice per week, and covers a range of launch times (Table 2).

The vertical resolution of the ozonesonde profiles (often > 2000 pressure levels) is reduced by interpolating the ozonesonde data onto 200 constant pressure levels from 1000 to 10 hPa. For comparisons, the model data are selected for the closest hour to the launch hour and then the closest grid-box to the ozonesonde station location. Furthermore, the model output is interpolated from the native resolution to the 200 constant pressure levels to match the sonde resolution, as was done in Keller et al. (2021).

3.3 TOLNet ozone lidars

In addition to comparisons against sounding data, the capability of the NASA GEOS-CF model to simulate and forecast the impact of stratospheric O_3 on tropospheric atmospheric composition can be assessed by comparing the GEOS-CF model output to observations from TOLNet. TOLNet is a network of 8 tropospheric O_3 lidars distributed throughout North America supported by NASA and NOAA (`https://www-air.larc.nasa.gov/missions/TOLNet`). These ground-based lidars provide Differential Absorption Lidar (DIAL)-derived, high vertical and temporal resolution, observations of tropospheric O_3 with high accuracy and precision continuously for many hours or even days (L. Wang et al., 2017; Leblanc et al., 2018). While Keller et al. (2021) found on average the NH free tropospheric O_3 was biased low compared to ozonesondes for 2018 to 2019, there is demonstrable synergy between the data from these lidar systems and the vertical structure of O_3 concentrations simulated by GEOS-CF (Dacic et al., 2020; Johnson et al., 2021), including episodic events when stratospheric O_3 descends to lower altitudes into the troposphere (Gronoff et al., 2021).

For this study, observations from the NASA JPL Table Mountain Facility (TMF) tropospheric O_3 lidar (TMTOL; McDermid et al., 2002), located in the San Gabriel Mountains near Los Angeles, California (34.38 °N, 117.68 °W) at an elevation of 2285 m above sea level (asl) are used. This system has the capability to conduct continuous observations for multiple hours or days (Chouza et al., 2019) providing O_3 measurements from 100 m above ground level (agl) to the tropopause. For a qualitative comparison to GEOS-CF for the case study in Section 5.3.3, the lidar data is averaged hourly with 30 m vertical resolution.

4 Model updates to GEOS-Chem UCX for GEOS-CF

Early evaluation of GEOS-CF v01 in 2018 against MLS observations indicated that GEOS-CF had significant biases in the stratosphere (not shown), caused by inaccurate initial conditions of ODSs as well as erroneous stratospheric removal of NO_x. Though the irregular stratospheric concentrations and distribution of some of the species had limited impact on the main observable tropospheric pollutants (Keller et al., 2021), it was critical that the state of the GEOS-CF stratosphere be addressed in order to be a suitable product for supporting NASA campaigns and remote-sensing instruments which require realistic stratospheric composition. To do so, parallel long-term free-running GEOS Chemistry Climate Model (GEOS CCM; Nielsen et al., 2017) simulations using the two troposphere-stratosphere chemistry mechanisms – GMI and GEOS-Chem – were performed to assess the GEOS-Chem stratospheric chemistry against the established GMI chemistry. This analysis confirmed that a well spun up GEOS-Chem stratosphere does lie within the observable total column O_3 range (Figure 1a).

From the comparison of these two long-term free-running GEOS CCM simulations, four major updates were made to the GEOS-Chem UCX code base in GEOS-CF to be more in line with the GMI mechanism since Eastham et al. (2014). In addition, two more changes were made to improve the O_3 nudging technique and the run-time performance.

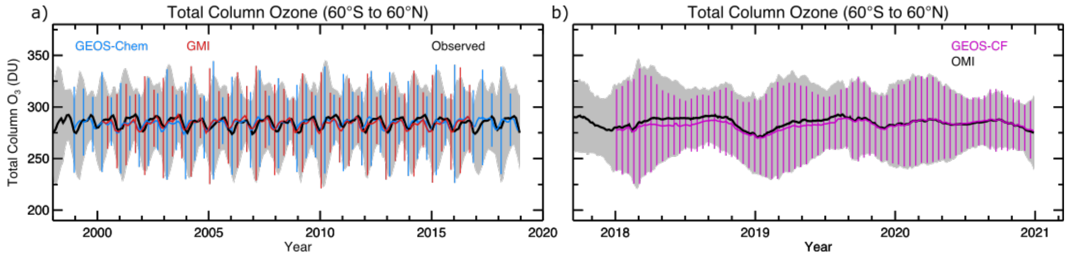

Figure 1. Near-global average (60 °S to 60 °N) TCO **(a)** monthly mean for the GEOS-Chem GEOS CCM free-running simulation (1999-2018; blue), GMI GEOS CCM free-running simulation (2000-2016; red), and the SBUV Merged O_3 Data Set (1998-2018, black). Vertical lines and grey shaded region represent the standard deviation about the monthly mean for the GEOS CCM simulations and observations, respectively, and **(b)** daily mean from OMI "TOMS-like" level 3 gridded product (McPeters et al., 2008; Bhartia, 2012, 7-day running mean, black line; std dev, grey shading) and GEOS-CF (7-day running mean, magenta line; standard deviation, magenta vertical lines) for the region from 60 °S to 60 °N.

Finally, the GEOS-CF stratospheric concentration fields were updated using the well-spun up (20-year) GEOS-Chem GEOS CCM simulation (blue line, Figure 1a). The updates and new initial conditions were implemented in the GEOS-CF near-real time system on 31 July 2019. The four major updates to the GEOS-Chem UCX code are:

First, the stratospheric photolysis and reaction rate constants were updated to follow recommendations provided by a more recent release of the JPL kinetic evaluation (JPL Publication 15-10; Burkholder et al., 2015) and the surface mixing ratio boundary conditions for ODSs were updated to follow the newer baseline emission scenario from the World Meteorological Organization (WMO) 2018 ozone assessment (Carpenter & Daniel, 2018). This update includes changing the methyl bromide (CH_3Br) boundary conditions to follow the WMO 2018 scenario rather than fixed zonal mean values (Parrella et al., 2012). Surface mixing ratio boundary conditions for N_2O in GEOS-CF are taken from the Representative Concentration Pathway (RCP) 6.0 scenario for the fifth assessment report of the Intergovernmental Panel on Climate Change (Collins et al., 2013). In addition to the halogenated source gases added by Eastham et al. (2014), the GEOS-Chem mechanism includes surface mixing ratios of brominated (Parrella et al., 2012) and chlorinated (Schmidt et al., 2016) very short-lived substances (VSLS) which were added to GEOS-Chem in versions 9.01.03 and 11.02, respectively. In GEOS-CF v01, the mean annual stratospheric total Cl and Br content for 2020 are 3.0 ppb and 19 ppt, respectively, in general agreement with the stratospheric supply estimated by Engel and Rigby (2018). The amount of Cl supplied to the stratosphere by tropospheric total inorganic Cl (Cl_y) and VSLS is minor, less than 2 %. Based on simulated mixing ratios at the tropical tropopause pressure, 5.6 ± 0.2 ppt of Br is supplied to the stratosphere by tropospheric Br_y and VSLS, in agreement with the previous modeling studies and aircraft observations summarized by the WMO 2018 Ozone Assessment (Engel & Rigby, 2018).

Second, more bromine was activated in GEOS-Chem than in the GMI simulations, contributing to greater O_3 loss in the lower stratosphere than observed, especially at low and mid-latitudes (see Figure 1b). Two heterogeneous reactions on polar stratospheric clouds (PSC) (reactions 1 and 2) and three reactions on stratospheric sulfate aerosols (reactions 1 - 3) were identified as not included in GMI and subsequently turned off in GEOS-CF. These reactions are:

$$ClONO_2(g) + HBr(l,s) \rightarrow BrCl + HNO_3 \tag{1}$$

$$HOCl(g) + HBr(l,s) \rightarrow BrCl + H_2O \quad (2)$$

$$BrONO_2(g) + HCl(l,s) \rightarrow BrCl + HNO_3 \quad (3)$$

The heterogeneous reaction 1 between chlorine nitrate ($ClONO_2$) and hydrogen bromide (HBr) on PSC surfaces was investigated by Hanson and Ravishankara (1992), but this reaction is disabled in the GEOS-CF system to be consistent with the GMI mechanism. Additionally, Burkholder et al. (2015) recommends that additional studies are needed to properly represent reaction 2, and laboratory analysis suggests that bromine nitrate ($BrONO_2$) and HCl do not directly react via reaction 3 (Hanson & Ravishankara, 1995). See Eastham et al. (2014) for details of the calculations of stratospheric sulfate aerosol and PSCs in GEOS-Chem UCX.

Third, the family transport of Cl_y and Br_y species is implemented in GEOS-CF as described by Douglass et al. (2004) for GMI. When halogen species are transported individually, Douglass et al. (2004) identified errors in the advection scheme along sharp gradients between sunlight and nighttime mixing ratios. These advection errors resulted in nonphysical maxima in mixing ratios of Cl_y and Br_y that were detected in earlier versions of the GEOS-CF stratosphere. Since the total quantities of Cl_y and Br_y do not have sharp day to night gradients, implementing family transport removes occurrences of non-physical maxima in halogen families in GEOS-CF v01.

Fourth, the solar zenith angle (SZA) in the photolysis calculations was updated to go beyond 90 degrees, thereby accounting for twilight conditions important for chemistry simulations in the stratosphere and mesosphere. GEOS-Chem version 12.0.1 and GEOS-CF now truncate the SZA at 98 degrees as done in GMI and allowed for in the Fast-Jx photolysis calculations. Previous versions of GEOS-Chem truncated the SZA at 90 degrees, which resulted in longer nighttime conditions and sharpened the day-night constituent gradients across the terminator. This contributed to the non-physical advection errors in the Br_y and Cl_y species described above.

In addition to the new initial conditions for GEOS-CF stratospheric concentration fields using the well-spun up (20-year) GEOS-Chem GEOS CCM simulation, two more adjustments were made to the GEOS-CF v01 system: (1) the start of the transition layer for the O_3 nudging was raised from GEOS level 38 (approximately 90 hPa) to GEOS level 35 (approximately 56 hPa as described in Section 2) in order to make sure no stratospheric O_3 was mistakenly added to the upper-troposphere since the nudging method does not differentiate between the stratosphere and troposphere; and (2) in the original version of GEOS-CF, GEOS-Chem UCX does explicit chemistry up to the stratopause and mesospheric chemistry is parameterized based on pre-defined production and loss rates. To speed up the run time of the GEOS-CF system, the mesospheric parameterization was disabled and stratospheric chemistry now extends up through the top of the GEOS atmosphere, thus avoiding the need to repeatedly read in production and loss rates. Note, this study is only evaluating stratospheric composition, considering concentrations up to 1 hPa.

For the evaluation of the GEOS-CF stratospheric composition in the following sections the focus is on only the 12-month period in 2020, after allowing several months for the stratosphere to stabilize. One can see an improved agreement in the (non-polar) total column O_3 between GEOS-CF and OMI from late 2019 onwards in Figure 1b. Prior to the inclusion of the above outlined updates on July 31, 2019, GEOS-CF mean non-polar total column O_3 is biased-low, and any analysis of the total column diagnostics or 3D stratospheric output from GEOS-CF v01 for this earlier period of the record should consider the potential biases from the stratospheric portion of the column.

It is unlikely that changes to atmospheric composition in 2020 from the COVID-19 pandemic restrictions impacted stratospheric composition significantly. For this reason, it is suitable to focus on the year 2020 for this study. Numerous studies investigated how the global COVID-19 pandemic restrictions impacted surface air quality through a reduction in anthropogenic emissions (an extensive collated list available at `https://amigo.aeronomie.be/index.php/covid-19-publications/peer-reviewed`); however, there are relatively few which explore the impact on free tropospheric (FT) composition – e.g., Steinbrecht et al. (2021) and Clark et al. (2021) report moderate decreases of 7 % NH FT O_3 for April to August 2020 and up to 12 % in FT O_3 over Frankfurt during March to July 2020, respectively – and no studies to our knowledge with a focus on the stratosphere. While a reduction in air traffic from the grounding of a substantial portion of passenger aircraft (Le Quéré et al., 2020; Clark et al., 2021) likely led to a decrease in emissions at cruising altitudes in the upper troposphere and lower stratosphere (UTLS), the anomalous NH springtime O_3 in the stratospheric polar vortex is likely a greater driver in UTLS composition anomalies than the pandemic-related emission reductions (see Figure 3, Steinbrecht et al., 2021). The anomalous polar vortex circulation and chemistry in the NH (January - May 2020) and the SH (May - September 2020), both of interest to stratospheric chemists, will be discussed in detail throughout Section 5.

5 Evaluation of GEOS-CF Stratospheric Composition

In this section, the spatial distribution and variations for stratospheric O_3 (Section 5.1) and several species important for O_3 chemistry (Section 5.2) are evaluated against independent observations and related to the complexity of chemistry and emissions. Once the state of the GEOS-CF stratospheric composition with analyzed meteorology is established, applications of the GEOS-CF forecasts are presented (Section 5.3).

5.1 Ozone

Since the GEOS-CF stratospheric O_3 is constrained during the replay segment by the GEOS FP O_3 product which assimilates MLS, OMI and OMPS-NM O_3 observations, independent profile observations from ozonesondes, ACE-FTS and SAGE III/ISS are used for validation with a comparison to MLS included.

In general, the median stratospheric O_3 simulated in GEOS-CF for the period between January through December 2020 agrees well with the median ozonesonde profiles (Figure 2) with median percent bias within $\pm$ 20 % through most of the stratosphere (Figure 3). While Alert and Eureka are located close to each other in northern Canada (see Figure S1), the median profiles between 150 to 30 hPa are very different for these two stations. This is attributed to the reduced number of profiles in 2020 for Alert compared to Eureka (17 and 65, respectively, Table 2), since this difference is not present when all profiles from 2018 to 2020 are considered (not shown). In addition, while Suva has the fewest profiles (15; Table 2) and exhibits a similar profile to its closest neighboring site Pago Pago (Figure 2) it has the largest median percent bias of all the profiles (> 80 % at 100 hPa; Figure 3). Furthermore, at the SH locations (King's Park to South Pole), there is a high bias in GEOS-CF median O_3, most notably between about 200 to 50 hPa (Figures 2-3). This is consistent with Stauffer et al. (2019), who assessed the "MERRA2-GMI" product (GEOS CCM with GMI replayed to MERRA-2 meteorology; Strode et al., 2015) against ozonesondes for the period 1980 to 2016 and found the subtropical and tropical sonde locations had median percent bias over 20 % between 15 to 20 km, and as they note, the median percent biases are large but the O_3 concentrations at these altitudes are low. Stauffer et al. (2019) also present a high bias for the MERRA2-GMI at SH high latitude sites between 10 to 15 km. Here, the differences between GEOS-CF and the SH polar observations at Syowa and South Pole in 2020 are driven by the model not capturing the low O_3 values in this layer of the atmosphere (between about 200 and 50 hPa, 25th percentile, dashed pink line, Figure 2) during austral winter and spring (individual months not shown). Possible reasons for biases in the SH polar regions in 2020 as it relates to polar chemistry are explored later in Sections 5.2 and 6.

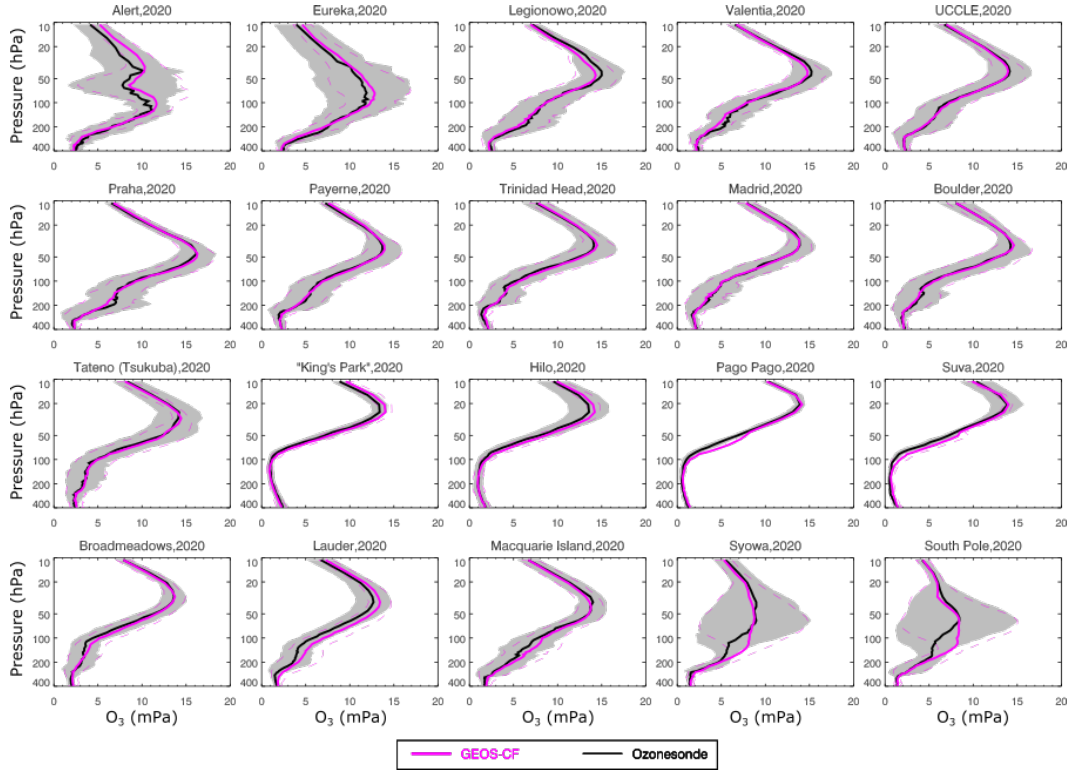

Figure 2. Median ozonesonde profiles (O_3, mPa) restricted to pressure levels between 400 to 10 hPa at 20 global stations for launches in January to December 2020 (median, black line; interquartile range, grey shading) compared to median GEOS-CF O_3 profiles (median, magenta solid line; interquartile range, magenta dashed lines). GEOS-CF profiles selected for the grid-box and time closest to the ozonesonde measurements. Launch locations displayed in order from North to South, as listed in Table 2.

Stratospheric O_3 in GEOS-CF also agrees well with SAGE III/ISS solar occultation profiles between 100 and 4.6 hPa for January through December 2020 with correlations coefficients (r) ≥ 0.92 (Figure 4 inset). At higher altitudes, near the stratopause at 1 hPa, the correlation is reduced, r = 0.61, with SAGE III/ISS reporting higher concentrations of O_3 than simulated by GEOS-CF (Figure 4). This bias may be a result of the SAGE III/ISS observations occurring near twilight and within 1.5 hours of the model times at altitudes where chemical time scales are short, and previous literature advised using caution for SAGE profiles outside the stratosphere (Damadeo et al., 2018; Davis et al., 2020; McCormick et al., 2020; H. J. R. Wang et al., 2020). However, the annual mean MLS O_3 is also slightly higher than mean GEOS-CF O_3 between 5 to 1 hPa globally, although still within the approximate instrumental 1σ uncertainty (Figure 5a-e). The annual zonal mean O_3 distribution for ACE-FTS is greater than GEOS-CF throughout most of the stratosphere, with the maximum difference located near the stratospheric O_3 concentration peak (Figure 5f-h); the negative bias is expected as ACE-FTS has a known positive bias to coincident MLS profiles (Dupuy et al., 2009; Sheese et al., 2017, 2021; Errera et al., 2019).

As demonstrated by this evaluation against independent observations, GEOS-CF realistically simulates stratospheric O_3 distributions between about 100 and 5 hPa. In the upper stratosphere (5 to 1 hPa), the disagreement between GEOS-CF simulated O_3 and satellite observations (SAGE III/ISS and MLS) will require further investigation but

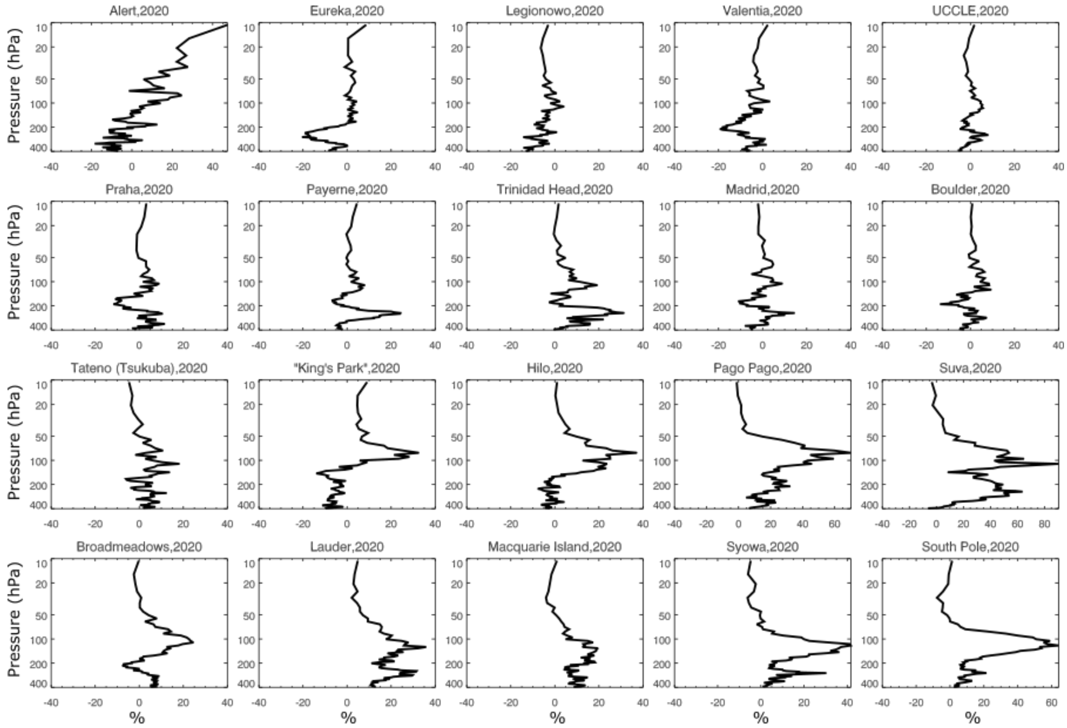

Figure 3. Similar to Figure 2, except median percent bias (GEOS-CF minus ozonesonde divided by ozonesonde). Note, x-axis range is generally from -40 to 40 % except at Pago Pago, Suva, and South Pole.

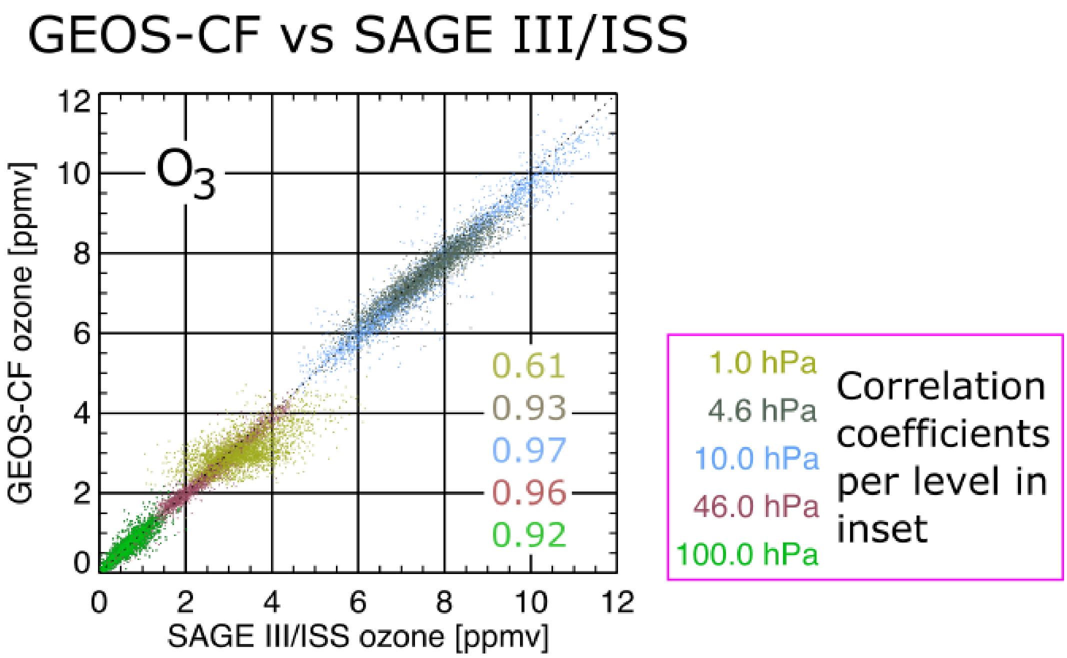

Figure 4. SAGE III/ISS solar occultation O_3 profiles for January to December 2020 interpolated to five MLS pressure levels – 100, 46, 10, 4.6, 1 hPa – and compared to GEOS-CF O_3.

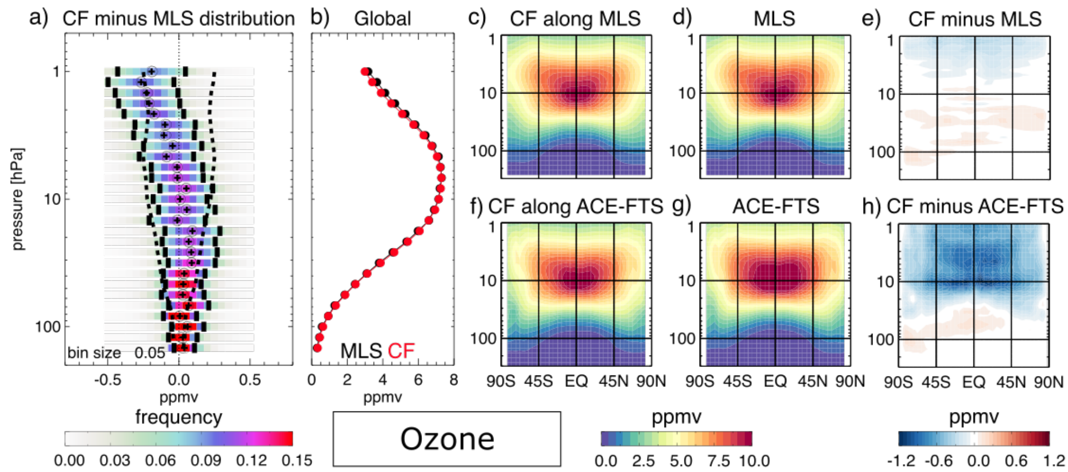

Figure 5. **(a)** PDF of the differences of GEOS-CF ("CF") O_3 minus MLS O_3 at 27 MLS pressure levels, with mean difference (open circle), median difference (cross), 1σ standard deviation (long dash), and approximate instrument 1σ uncertainty from the MLS quality document tables (short dash). **(b)** the mean concentrations for GEOS-CF (red) and MLS (black) at 27 MLS pressure levels from 146.8 to 1.0 hPa. For **(a,b)**, only MLS data within half an hour of the synoptic times (0, 6, 12, 18 UTC) are used for January to December 2020. **(c,f)** Zonal 2020 annual mean O_3 for GEOS-CF co-located to the satellite overpasses, **(d,g)** the zonal 2020 annual mean O_3 for the satellite and **(e,h)** the difference of the model minus the satellite for **(c-e)** MLS and **(f-h)** ACE-FTS.

is likely associated with the extension of stratospheric chemistry up to the mesosphere. The positive bias in GEOS-CF O_3 in the SH polar region between about 200 to 50 hPa present in the comparisons against ozonesondes (Figure 2) and satellite observations by both MLS and ACE-FTS (Figure 5e,h) will also be monitored closely.

5.2 Chemical species important to stratospheric O_3 chemistry

Next, comparisons of the model against satellite observations are presented for stratospheric species that are relevant to polar vortex chemistry and observed by both MLS and ACE-FTS, including two inorganic chlorine species (HCl and ClO), two nitrogen species (HNO_3 and N_2O), and additional nitrogen species only observed by ACE-FTS. GEOS-CF outputs MLS observed species on approximate MLS pressure levels; the ACE-FTS observations were interpolated to these GEOS-CF "MLS pressure levels". For the additional chemical species which are not reported by MLS but are reported by ACE-FTS, the GEOS-CF 3D 3-hourly, instantaneous output on 35 isentropic surfaces (from 270 to 3000 K) are compared to ACE-FTS measurements. The ACE-FTS observations were interpolated to isentropic surfaces from 330 to 1600 K for the comparison and the GEOS-CF isentropic output within 1.5 hours of the ACE-FTS measurements are selected.

5.2.1 Inorganic chlorine

Inorganic chlorine in the stratosphere is the result of transport of tropospheric long-lived chlorine compounds, most notably chlorofluorocarbons (e.g., CFC-11 (CCl_3F) and CFC-12 (CCl_2F_2)), chlorinated solvents (e.g., carbon tetrachloride (CCl_4)) and methyl chloride (CH_3Cl). Once in the stratosphere, the long-lived compounds photolyze and react with other chemical species (in the presence of UV) to form reactive chlorine, which through catalytic cycles can lead to loss of stratospheric O_3 (Molina & Rowland, 1974b, 1974a). The CFCs and CCl_4 are the result of industrial activities and other man-made products which have been phased out following the Montreal Protocol and subsequent amendments (Reimann et al., 2018). CH_3Cl originates mainly from natural sources such as biomass burning emissions, the ocean, and fungi (Keene et al., 1999).

It is critical for the GEOS-CF forecast capabilities of stratospheric O_3 that species such as these are simulated correctly. Several other Cl_y species are observable from space, however, the focus is limited to 1) HCl, a non-ozone-destroying chlorine reservoir, and 2) ClO, an active, ozone-depleting chlorine radical (Stolarski & Cicerone, 1974). HCl is abundant in the stratosphere, especially at high altitudes, and as a reservoir species it is relatively inert. Because of the global distribution of these chlorine species, O_3 loss through catalytic cycles can occur throughout the stratosphere; however, this is usually at a slower rate compared to O_3 loss following the conversion of HCl and $ClONO_2$ (another chlorine reservoir) to ClO on PSCs (Solomon et al., 1986) within a sunlit wintertime polar vortex. When polar stratospheric temperatures begin to drop as the vortex forms, the environment becomes favorable for the formation of PSCs. While the maintenance of extremely cold temperatures is more common in the austral winter and spring polar vortex, during the 2020 boreal winter and spring a stable polar vortex led to PSCs which were observed by the OMPS Limb Profiler (LP) (DeLand et al., 2020). Within the polar vortex, the heterogeneous chemistry can lead to substantial destruction of stratospheric O_3. This is demonstrated in the snapshot of the NH polar vortex on 29 February 2020 at 22 UTC, comparing GEOS-CF simulated concentrations to measurements from a single MLS overpass (Figure 6). As stated in Section 5.1, it is no surprise that the NH O_3 agrees well to MLS in Figure 6a since GEOS-CF at 45 hPa is nudged toward the GEOS FP assimilated product. Presented here is how GEOS-CF simulates the location and chemistry of the vortex; although, GEOS-CF underestimates the observed high values of HCl outside the vortex (Figure 6b) and the highest ClO values within the sunlit portion of the vortex (Figure 6c) as seen by MLS.

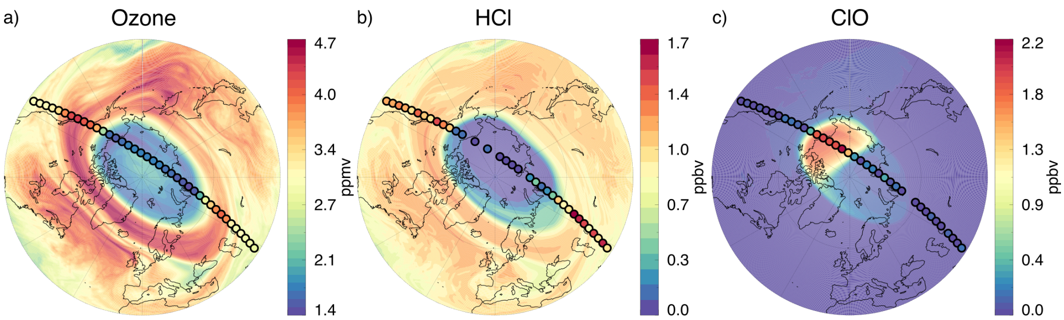

Figure 6. Snapshot of 29 February 2020 at 22 UTC for GEOS-CF (map) versus a single overpass of MLS (colored circles; measurements from 21:43 UTC to 22:14 UTC) at 45 hPa for **a)** O_3, **b)** HCl and **c)** ClO, emphasizing the NH polar vortex chemistry.

Figure 6 is only an example on one pressure level (45 hPa), but it is an accurate representation of the global distribution further investigated in Figures 7 and 8. First, the annual global distribution of HCl from the model is compared against MLS and ACE-FTS profiles of HCl in Figure 7. Throughout the stratosphere, GEOS-CF simulates the vertical gradient of increasing HCl concentrations from the lower stratosphere to upper stratosphere as seen by the satellite measurements. However, the model is biased low compared to the 2020 observations. This holds true at all latitudes except in SH polar region in the lower stratosphere when compared against ACE-FTS measurements where

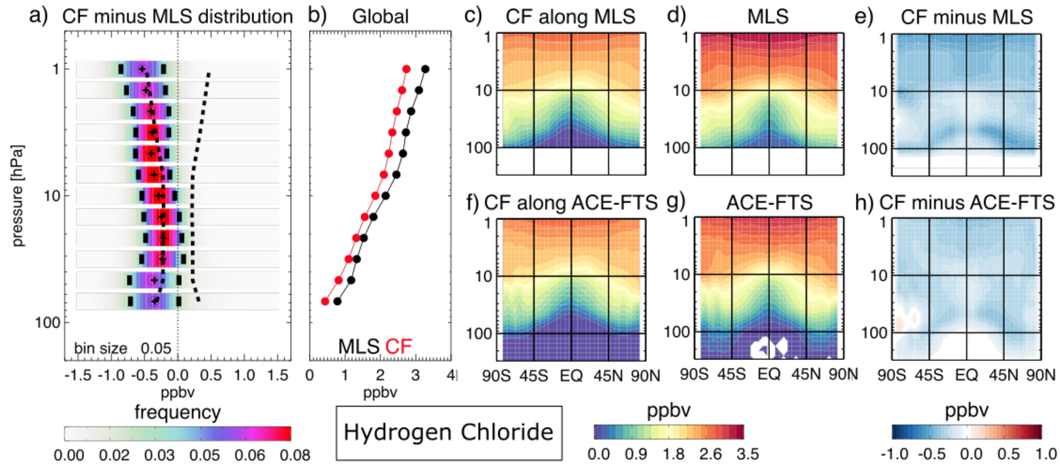

Figure 7. Similar to Figure 5 but for HCl and only MLS data within half an hour of 12 UTC for January to December 2020. Negative values from ACE-FTS are colored white (**g**).

there is a positive difference (100 to 50 hPa; Figure 7h). The positive bias in ACE-FTS, which is not seen in the annual zonal difference between GEOS-CF and MLS, is likely due to a sampling bias by ACE-FTS. The SCISAT orbit is such that ACE-FTS has sunrise measurements south of 60 °S only during a few months a year (March, April, July, early August, and November; `https://ace.uwaterloo.ca/mission_orbit.php`). During July and August, there are positive biases between GEOS-CF and MLS in the SH lower stratosphere (top, Figure S2), however, there is a large negative bias in late 2020 between GEOS-CF and MLS (Figure S2) that likely cancels out the mid-year positive biases seen in the SH high latitudes. There is also a bias between ACE-FTS and GEOS-CF $ClONO_2$ (Figure S4), which may indicate that the Cl_y loading is low in the model.

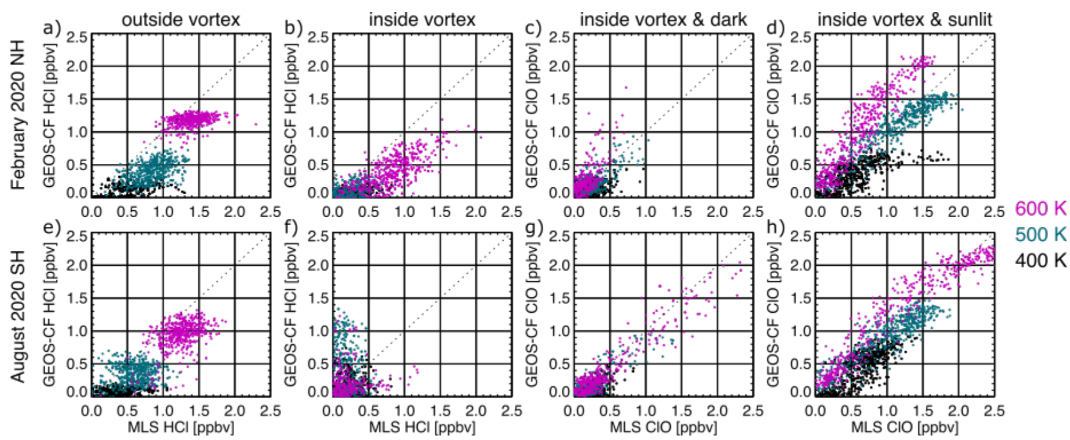

Figure 8. Scatter plots of GEOS-CF (y-axis) versus MLS (x-axis) for HCl (left) and ClO (right) for NH February 2020 polar vortex (top) and SH August 2020 polar vortex (bottom). Outside vortex is defined as from 30° N or S to the vortex edge. The vortex edge is defined as in Wargan, Weir, et al. (2020).

Second, to look at the vortex chemistry in more detail, the polar distributions of HCl and ClO during February 2020 (NH only; Figure 8a-d) and August 2020 (SH only;

Figure 8e-h) for three isentropic surfaces (400, 500 and 600 K) are compared for GEOS-CF against MLS. For the model to correctly simulate the O_3 destruction within the vortex, there needs to be an accurate representation of the heteorogenous processes. Within the polar vortexes (NH and SH), concentrations of HCl both observed by MLS and simulated by GEOS-CF decreased compared to outside the vortex (Figure 8); however, GEOS-CF simulated HCl is biased high (low) within the SH (NH) vortex for August 2020 (February 2020) compared to MLS. It is on the PSCs that the chlorine reservoir species are converted to ClO through heterogeneous processes in the presence of sunlight (Figure 8). Within the polar vortexes of 2020, GEOS-CF simulates the increase in ClO abundance within the sunlit portion, although GEOS-CF is biased high with respect to MLS at higher altitudes where there is also a low bias in simulated HCl (600 K, Figure 8d,h), likely indicating too much chlorine was activated. Since global distributions of ClO are very low outside of the sunlit portion of the vortex, a comparison on the global scale, similar to Figure 7, was not performed.

5.2.2 Nitrogen Family

Another catalytic cycle for stratospheric O_3 loss is with nitrogen oxides (NO_x = $NO + NO_2$). In the stratosphere, N_2O is the main source for NO and subsequently other nitrogen species collectively referred to as NO_y. We define NO_y as the sum of major reactive nitrogen species: $NO + NO_2 + HNO_3 + ClONO_2 + 2*N_2O_5$. A long-lived greenhouse gas, N_2O has natural and anthropogenic sources in the troposphere with no significant sinks until reaching the stratosphere. Once in the stratosphere, N_2O dissociates through photolysis and reaction with excited oxygen atoms to produce NO and is thus a major source of stratospheric NO_y (Crutzen, 1970). During the night time, some NO_2 is converted to N_2O_5, which acts as a reservoir species for NO_x until the sunlight returns. The reaction of ClO with NO_2 forms $ClONO_2$ (Rowland et al., 1976), and $ClONO_2$ is a reservoir species for both reactive chlorine and nitrogen. HNO_3, another nitrogen reservoir, is formed by the reactions of NO_2 with the hydroxyl radical (OH) and through heterogeneous reactions with N_2O_5, and HNO_3 later photolyzes to return OH and NO_2 to the system (Brasseur & Solomon, 2005).

The annual zonal mean distributions of N_2O, NO_x and NO_y in GEOS-CF are compared against measurements from ACE-FTS in Figure 9. While N_2O measurements are available from both MLS and ACE-FTS, profile measurements of NO_x are only available from ACE-FTS and there is a known bias in MLS N_2O measurements in the lower stratosphere (Livesey et al., 2021). The expected N_2O distribution based on the known sources and sinks can be clearly seen in Figure 9 (see also Figure S3 for MLS and ACE-FTS on pressure levels), with the largest concentrations in both the model and the satellite at lower altitudes (closer to tropospheric sources) as well as reaching higher altitudes near the equator because of strong upwelling into the stratosphere over the tropics. At concurrent sampling of GEOS-CF to ACE-FTS measurements, the N_2O spatial patterns for the model and satellite in the stratosphere are consistent, although the model is biased low through much of the stratosphere (isentropic levels up to 1100 K) and biased high in the upper stratosphere (1200 to 1600 K), particularly in the tropical region (Figure 9; see also from 50 to 5 hPa and 5 to 1 hPa in Figure S3f-h for similar difference patterns in comparison to MLS N_2O).

To reduce the potential errors because of mismatches around twilight between the GEOS-CF gridpoint and the ACE-FTS measurements, we included N_2O_5 with NO_x as "NO_x*" to estimate the full diurnal cycle of NO_x in Figure 9d-f. For both the satellite and GEOS-CF, there is a maximum in NO_x* (15 and 18 ppbv, respectively) in the tropical upper stratosphere (around 1200 to 1400 K) and concentrations decrease toward the higher latitudes. NO_x converts to HNO_3 and $ClONO_2$ in the middle stratosphere over mid-latitudes, a process that can be seen in Figure 9d-e where higher NO_x* stems towards lower isentropes and higher latitudes, into the region of maximum NO_y (Figure 9g-

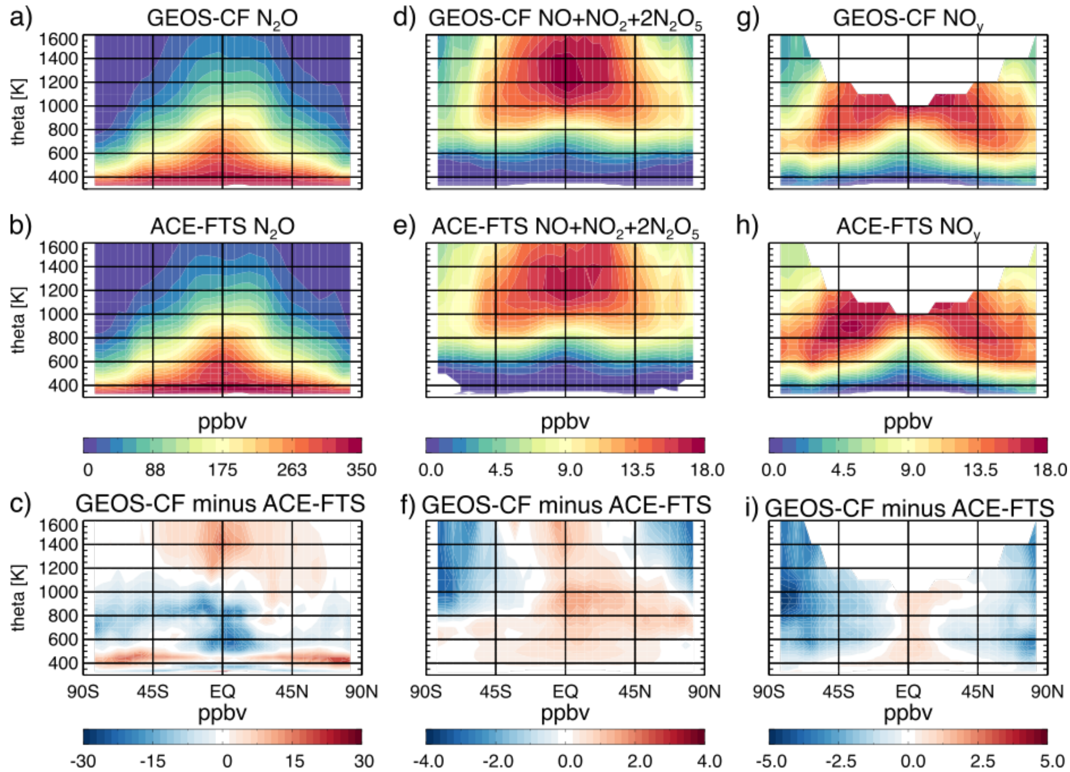

Figure 9. Zonal annual means for GEOS-CF (top row) and ACE-FTS measurements (middle row) and the difference of GEOS-CF minus ACE-FTS (bottom row) for N_2O (left), "NO_x" ($NO + NO_2 + 2*N_2O_5$; middle), and NO_y ($NO + NO_2 + HNO_3 + ClONO_2 + 2*N_2O_5$; right) for isentropic levels from 330 to 1600 K. Note, ACE-FTS does not measure $ClONO_2$ at high altitudes so missing values of NO_y are white.

h; see also Figure 11 for HNO_3 only distributions and Figure S4 for NO_y partitioning for ACE-FTS and GEOS-CF).

Since the production of N_2O in the stratosphere is insignificant, it is an ideal tracer for evaluation of model transport (e.g., Strahan et al., 2007; Jin et al., 2009; Manney et al., 2009; Ruiz et al., 2021). While the individual nitrogen species in NO_y are not long-lived, together they can be considered as a long-lived tracer. Generally, NO_y mixing ratios increase and N_2O decrease as air ages in the stratosphere (see Figure 9); thus, compact relationships form between NO_y and N_2O due to transport and isentropic mixing (e.g., Chang et al., 1996; Koike et al., 2002; Wetzel et al., 2002; Plumb, 2007). Since in the stratosphere air parcels generally move adiabatically, it is useful to explore these relationships using isentropic surfaces (i.e., constant potential temperature). In Figure 10, values of stratospheric NO_y are shown relative to N_2O with colors representing the potential temperature of the individual non-polar points and black for all polar points. Concentrations of N_2O are the highest near the tropospheric sources, seen in both ACE-FTS and GEOS-CF at low potential temperature levels. The relationship between N_2O and NO_y is comparable between the satellite and model as air enters the lower stratosphere from the troposphere and ages as it moves upward (to higher potential temperature levels), evidence that GEOS-CF has realistic transport in the lower to middle stratosphere ($N_2O > 100$ ppbv).

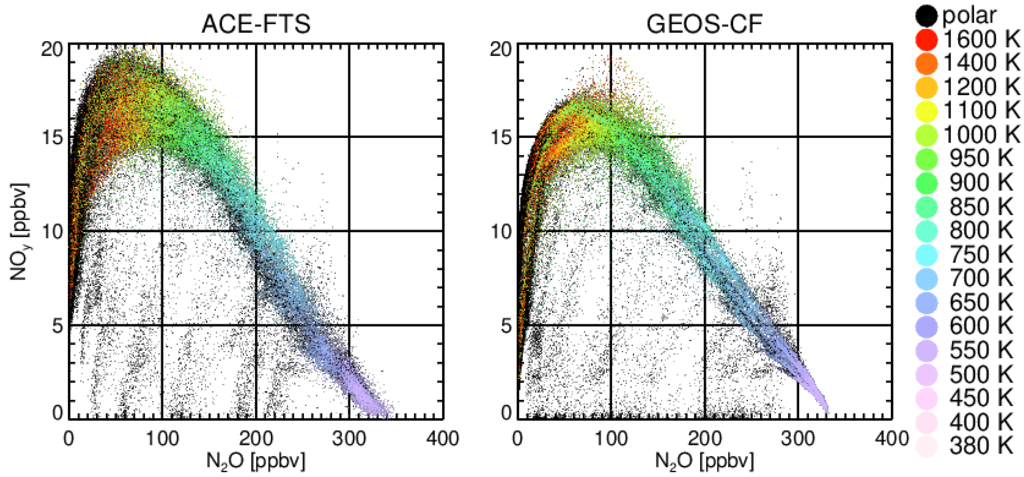

Figure 10. NO_y ($NO + NO_2 + 2N_2O_5 + HNO_3 + ClONO_2$) versus N_2O for ACE-FTS (left) and co-located GEOS-CF (within 1.5 hours, as in Figure 9; right) colored by potential temperature from 380 K to 1600 K for latitudes from ± 60°, polar observations are black.

However, GEOS-CF does not capture the spread of high values of NO_y (> 15 ppbv) observed by ACE-FTS in the stratospherically aged air (i.e., mixing ratios of N_2O < 100 ppbv). When the air reaches the upper stratosphere (warm colors in Figure 10, N_2O < 100 ppbv) and polar regions (black dots in Figure 10 indicate > |60°|), the tracer-tracer relationship is no longer linear. In the upper stratosphere, chemical processing of NO_y takes place faster than the timescales of the stratospheric transport, as evidenced by the drop off in NO_y as N_2O mixing ratios decrease below 100 ppbv. Similarly, the observed and simulated low values of NO_y and N_2O below the main tracer-tracer curve (black points in Figure 10) suggest that GEOS-CF properly represents the polar vortex mechanisms that remove NO_y from the system until NO_y-rich air from the mid-latitudes replenishes the polar regions after the break-up of the vortex. The NO_y depleting mechanisms that take place within the polar vortex include reversible 'denoxification' (removing NO_x from the gas phase) and irreversable 'dentrification' (sedimentation of HNO_3-containing PSCs; Salawitch et al., 1989; Toon et al., 1990).

Isolating HNO_3 from NO_y is portrayed in Figure 11. In GEOS-CF, the mid- to high latitude maxima of HNO_3 are simulated correctly in the lower stratosphere between 100 to 10 hPa, where the photochemical lifetime of HNO_3 is long, however the concentrations are not as large as observed by MLS or ACE-FTS (Figure 11c-h). The general low bias in simulated HNO_3 compared to MLS observations is within the lower limit of the instrument uncertainty estimate (as indicated by the dotted lines in Figure 11a). Near the poles, concentrations of HNO_3 decrease (Figure 11c-d,f-g) through denitrification. The spread of the N_2O:NO_y polar points below the majority of the points in Figure 10 indicates that the model is simulating denitrification similar to ACE-FTS measurements.

In order to inform future model development, we hypothesize some possible reasons for the biases in nitrogen species related to chemistry and emissions that should be considered in future versions of GEOS-CF.

In the polar regions, there are a negative differences between ACE-FTS and GEOS-CF NO_x* in the upper stratosphere and throughout the polar stratosphere for NO_y. This may be linked to missing sources of mesospheric NO_x. One such source is in the thermosphere whereby energetic electrons from galactic cosmic rays react with molecular ni-

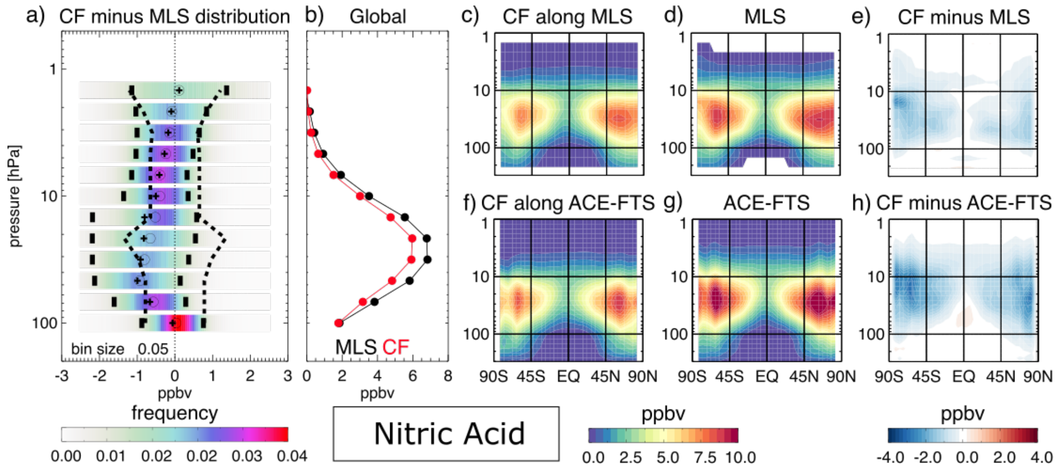

Figure 11. Similar to Figure 7 but for HNO_3.

trogen (N_2) to produce atomic nitrogen (N) in either excited $N(^2D)$ or ground $N(^4S)$ state that can then react with molecular oxygen (O_2) or OH to produce NO (e.g., Solomon et al., 1982; Siskind et al., 1997). There is evidence that some of this NO can be transported down into the mesosphere and stratosphere, especially in the polar regions where there is downwelling in the mesosphere, and concentrations should be higher as it is not photochemically destroyed during polar night (Randall et al., 2005, 2007; Funke et al., 2005). This missing source from galactic cosmic rays has been identified in another modelling study to explain some of the discrepancies in chlorine and nitrogen species associated with the SH winter and spring polar vortex when compared against satellite observations (Grooß et al., 2018). Sources of mesospheric NO_x are not represented in the GEOS-CF system and may be further confounded by the extension of stratospheric chemistry into the mesosphere in GEOS-CF (see Section 2). Furthermore, when each month is assessed individually, from April 2020 to August 2020, the SH stratospheric low HNO_3 bias decreases in the same region as the high bias in HCl (Figure S2) while the biases in both HCl and HNO_3 increase along the vortex edge instead of in the vortex center during winter time in keeping with the findings of Grooß et al. (2018) for HCl. A future version of GEOS-CF may benefit from upper-boundary emission sources representing the solar and galactic high energy particles as diagnosed by Grooß et al. (2018).

In the equatorial stratosphere there is a positive bias in $NO_x{}^*$ and NO_y between the model and ACE-FTS (Figure 9f and i). As stated in Keller et al. (2021), GEOS-CF uses the unadjusted lightning parameterization (described in Murray et al., 2012) which leads to higher lightning NOx in the tropics. However, this is likely a very small contribution to the positive difference seen in the equatorial region between observations and model in Figure 9. Another theory is the positive bias of N_2O above the large negative bias in the tropics (Figure 9c) may indicate that the vertical transport is too fast, however the model generally captures the observed distributions of nitrogen-containing species (Figure 9a,b) and the N_2O to NOy relationship in the lower to mid-stratosphere (Figure 10), both indicating that GEOS-CF correctly captures the large-scale transport pathways (Holton, 1986; Mahlman et al., 1986). Instead of transport, the biases may be due to chemistry. Higher in the equatorial stratosphere, the GEOS-CF maximum in $NO_x{}^*$ is larger in magnitude and extends to higher potential temperature surfaces than observed by ACE-FTS (Figure 9d-e). The positive bias in GEOS-CF $NO_x{}^*$ is in a similar location as the positive bias in N_2O. With the increased available N_2O, production of $NO_x{}^*$ may be greater in the upper stratosphere than is observed. Also, the conversion to other nitrogen species, such as HNO_3, may be too slow, as indicated by NO_y partitioning (Figure S4).

5.3 Stratospheric O_3 Forecast Capability

In Sections 5.1 and 5.2, the state of the stratospheric composition for GEOS-CF when the model is constrained by observed meteorology was characterized. In this section, a few case studies explore the skill of the GEOS-CF model during the five-day forecasts when the meteorology is free-running. First, the evaluation of five-day forecasts for the NH and SH anomalous polar events using GEOS-CF and GEOS FP against the NASA Ozone Watch merged satellite product is presented. The year 2020 highlighted some aspects of stratospheric O_3 interannual variability which occur because of both atmospheric dynamics and chemistry. In particular, during the boreal winter to spring, the relatively undisturbed stratosphere allowed the NH polar vortex and associated anomalously low polar O_3 to persist (Inness et al., 2020; Lawrence et al., 2020; Manney et al., 2020; Wohltmann et al., 2020; Dameris et al., 2021). A similar situation existed in the late austral winter and spring, where, as will be shown below the strongly zonal stratospheric winds allowed the SH ozone hole to extend longer than normal (Lecouffe et al., 2021). Thus, in both time periods, polar O_3 column values were generally far below their climatological values, highlighting the need during these times for O_3 chemistry forecasts based on full stratospheric O_3 chemistry (e.g., GEOS-CF) rather than parameterized chemistry (e.g., GEOS FP) which can be based on average production and loss rates or an O_3 climatology. GEOS-CF forecasts are first described for the 2020 NH anomalous event for the total O_3 column in the 63 to 90 °N polar cap (Section 5.3.1), followed by forecasts for the area of the 2020 SH ozone hole size as measured by the total O_3 column less than 220 DU (Section 5.3.2).

Another application of the GEOS-CF forecasts is the ability to provide the air quality community with realistic five-day forecasts of stratospheric intrusion events, when stratospheric O_3-rich air is irreversibly mixed into the troposphere, which can lead to O_3 air quality exceedances events especially at high altitude locations. This new capability is highlighted in Section 5.3.3 (see also Duncan et al., 2021).

5.3.1 NH spring 2020 polar ozone anomaly

Record low NH polar cap O_3 occurred during January to April 2020 (Figure 12a; blue curve compared to black curve)(Lawrence et al., 2020; Inness et al., 2020) with the average value for March being approximately 75 DU (20 %) below climatology. During this time, the five-day GEOS FP forecast trajectories (gray curves) tended toward the higher climatological values (e.g., for March is on the order of 400-450 DU; Feng et al., 2021), as expected with simplified chemistry. On the other hand, the corresponding GEOS-CF trajectories (red curves) remained consistent with the future GEOS-CF initial values, as the sophistociated GEOS-Chem chemistry is able to simulate a more realistic atmosphere. The smaller GEOS-CF mean five-day bias (with respect to the concurrent GEOS-CF replay) for the four month period, -1.8 DU, compared to the GEOS FP bias (with respect to concurrent GEOS FP analyses), 8.7 DU, reflects this tendency (see inset, Figure 12a). The GEOS-CF mean behavior consistently tracked closely to the independently analyzed Ozone Watch values (blue contour). The closeness of the GEOS-CF and GEOS FP five-day forecast's standard deviation of the error, 2.7 and 4.1 DU respectively (see inset, Figure 12a), indicate that both systems realistically captured the day-to-day dynamically induced variations of polar cap O_3.

As a specific example, the GEOS-CF and GEOS FP forecast trajectories, initialized on 5 March 2020, evolved in different directions (Figure 12b). Since GEOS-CF is nudged toward the GEOS FP O_3, the forecasts start at a similar place; however, GEOS-CF and GEOS FP forecasted changes of -7.5 and 5.4 DU, respectively, over the five-days.

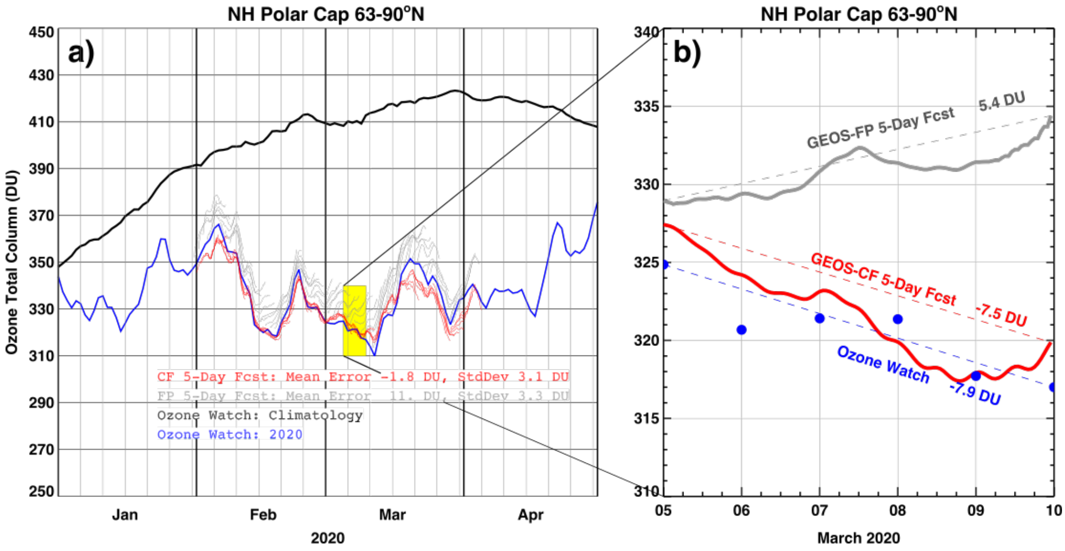

Figure 12. Total column O_3 (DU) for the NH Polar Cap region (63 to 90 °N) from GEOS-CF five-day forecast trajectories (red), GEOS FP five-day forecast trajectories (gray), Ozone Watch analysis (blue), and Ozone Watch 1979-2020 climatology (black) **a)** from January to April 2020 and **b)** from 5 March to 10 March 2020 for forecast initialized 12 UTC 5 March 2020. **a)** The thick vertical lines denote the first day of each month, while the light vertical lines denote five-day intervals starting from January 1, 2020. The yellow box indicates the period of the case study in **b)**. **b)** Date labels correspond to mid-point in the day (12 UTC).

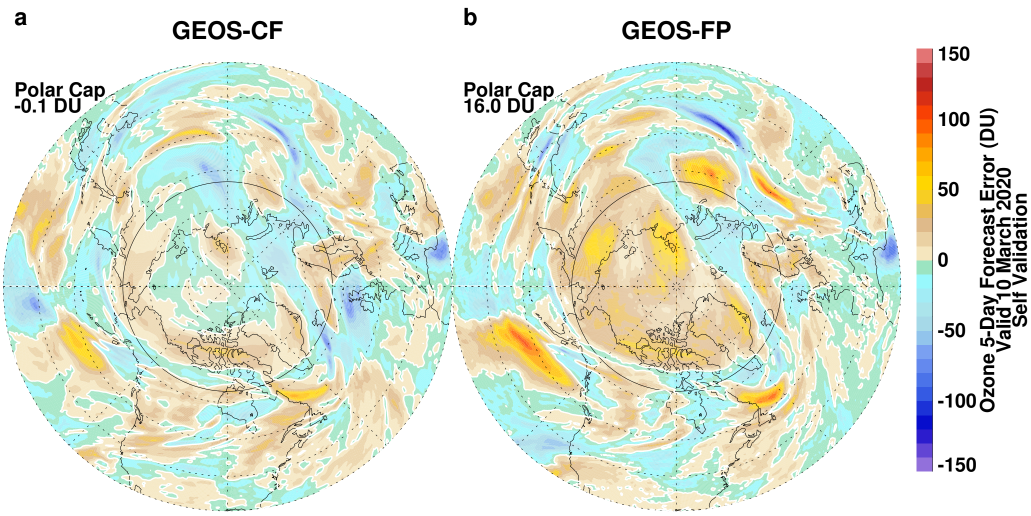

Figure 13. Total O_3 forecast error (DU) for 10 March 2020 calculated by the five-day forecast initialized on 5 March 2020 at 12 UTC minus the analysis (date the forecast is valid) from a) GEOS-CF and b) GEOS FP. Solid black circle indicates the 63°N latitude for the polar cap region of interest.

In this example, the GEOS-CF predicted polar cap O_3 decrease agreed well with the Ozone Watch analyzed change of -7.9 DU. Furthermore, a hemispheric view of the five-day forecast error for the 10 March 2020 (Figure 13) reveals a substantial increase over most of the polar cap in GEOS FP compared to the more random error pattern found in GEOS-CF. In addition to the errors in the polar cap, GEOS FP NH middle latitude O_3 column errors often peak higher than the corresponding GEOS-CF errors (Figure 13, red values).

5.3.2 SH 2020 Ozone hole area

The distinctive, long duration, 2020 ozone hole kept its area larger than the climatological average from early August until after November (blue line versus black line, Figure 14). The anomalous polar vortex conditions again push past the limits of the GEOS

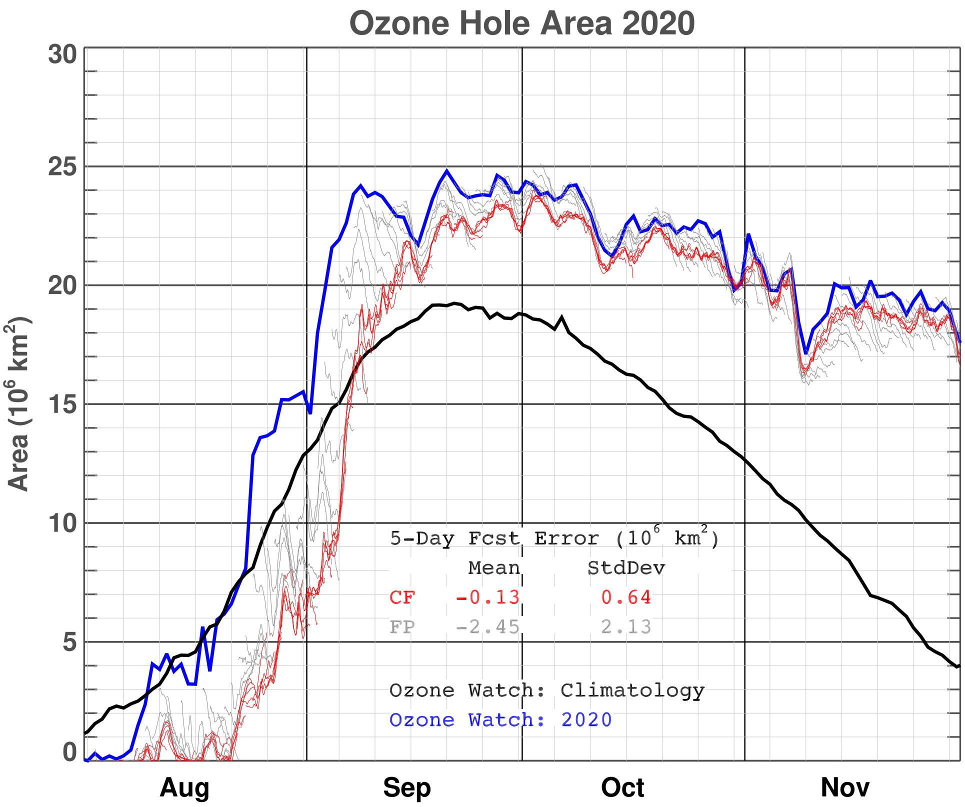

Figure 14. Similar to Figure 12a except for ozone hole area (10^6 km^2) from August to November 2020, with the five-day intervals starting from 1 August 2020.

FP O_3 forecasts with simple chemistry, as in the 2020 NH spring. Forecasting the ozone hole area during the development of the SH ozone hole in August proved difficult for both GEOS-CF and GEOS FP; since weak gradients near the 220 DU value exist at this time, it makes exact determination of the area difficult, which may influence the analysis uncertainty at this stage. In addition, the sunless August polar region limits coverage of solar backscatter satellite O_3 observations and therefore less observational constraints on the models' analyzed O_3. However, by the middle of September, the ozone hole area determined from the GEOS FP initial conditions (GEOS FP analysis, corresponding to the start of each gray line) and the GEOS-CF five-day forecast trajectories (start of each red line) agreed well with the O_3 Watch 2020 values.

As expected, the GEOS FP five-day forecasts tended toward a smaller ozone hole area, more characteristic of the climatological ozone hole area (black line, Figure 14; see also Figure 8 of Nielsen et al., 2017). Over the four month period and using self-validation (in units of 10^6 km^2), the GEOS FP fifth-day forecast bias (-2.45; see inset Figure 14) greatly exceeded in magnitude the GEOS-CF forecast bias (-0.13) and the GEOS FP error standard deviation (2.13) also exceeded that of GEOS-CF (0.64). Thus, despite not simulating the ozone hole area consistent with Ozone Watch at the onset in August, during the SH ozone hole of 2020 GEOS-CF successfully forecasted changes in the ozone hole area out to five-days.

5.3.3 Forecast capability for stratospheric intrusions

Stratospheric intrusions occur when the tropopause – the boundary between the stratosphere and troposphere – wraps around the jet core, bringing stratospheric air down toward the surface. This folding of the tropopause is generally associated with upper-tropospheric level troughs and cut-off lows. These synoptic weather patterns occur year round, however the tropopause folding events are of interest to air quality managers especially in the spring and early summer (March through June). During this time of year there is a maximum in O_3 in the lower stratosphere which is drawn down within a fold and the photochemical production of O_3 at the surface is not yet the dominant source of O_3 leading to air quality standard exceedances. Ott et al. (2016) and Knowland et al. (2017) both demonstrated that the GEOS model run at horizontal resolutions of 50 km or less with O_3 data assimilation can represent stratospheric intrusions which are linked with ground-level O_3 enhancements, however the tropospheric O_3 is biased from the simplified chemistry used in the GEOS forecast and reanalysis products prior to the inclusion of GEOS-Chem in the GEOS-CF system.

Tropospheric O_3 lidars have a demonstrated record of successfully measuring stratospheric intrusions (e.g. Langford et al., 2009; Kuang et al., 2012, 2017). Here one example of a large stratospheric intrusion event forecasted in near-real time by GEOS-CF to pass over NASA JPL's TMF (Figure 15) on 13 June 2020 as captured by TMTOL (Figure 16a) is examined. GEOS-CF indicated a potential O_3 enhancement above TMF that is likely of stratospheric origin (no disconnect with the atmosphere above 10 km) five-days in advance (Figure 15a). This feature was then present in each of the five-day forecasts at decreasing lag times (Figure 15b-e), indicating a high likelihood that it is a dynamic event and will be realized. At the location of TMF, GEOS-CF simulates both the high levels of stratospheric O_3 and the photochemically-produced O_3 enhancement transported from Los Angeles basin up to TMF (high levels of O_3 near the 2000 m altitude; Figure 15).

On 13 June 2020, the TMTOL operated throughout the day (Figure 16a). The GEOS-CF replay output (Figure 16b; originally on pressure levels and converted to altitude) simulates the two O_3 tongues around the time of enhancements seen by the TMTOL. While there are differences in the extent and timing of the O_3-rich air descending into the troposphere, this example highlights the strengths of the GEOS-CF's coupled stratosphere-troposphere chemistry in its ability to forecast the impact of stratospheric composition on tropospheric air quality.

6 Conclusions

NASA's GEOS Composition Forecast system (GEOS-CF; Keller et al., 2021) provides near real-time estimates of recent atmospheric composition with daily five-day forecasts at high spatial resolution (0.25° latitude x 0.25° longitude up to the lower mesosphere) and high temporal frequency (3D at hourly and 3-hourly intervals). GEOS-CF products are used to support ground-based, balloon, and satellite-based instrument teams, as well as field and aircraft campaigns that measure trace gases in the troposphere and

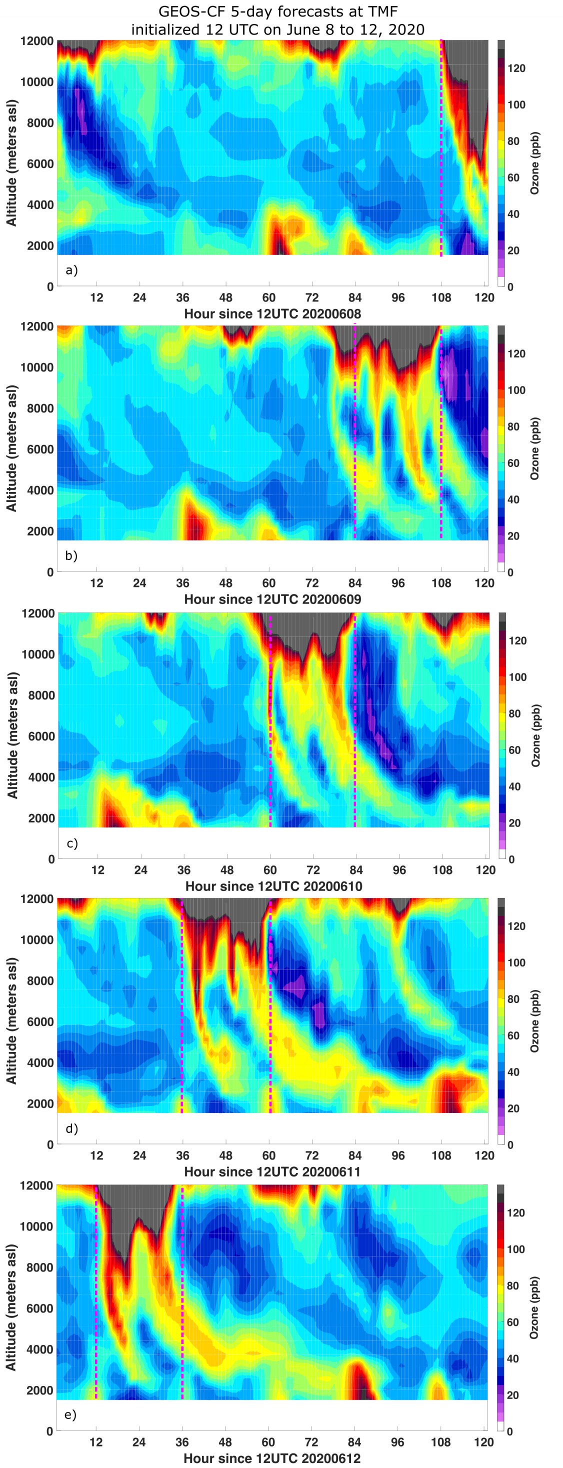

Figure 15. GEOS-CF five-day (120 hour) O_3 forecasts for grid box closest to TMF (34.25 °N, 117.75 °W) initialized at 12 UTC on a) 8 June 2020, b) 9 June 2020, c) 10 June 2020, d) 11 June 2020, and e) 12 June 2020. The GEOS-CF O_3 on 23 pressure levels from 1000 to 10 hPa are interpolated to altitude in meters asl for comparison to TMF observations (see Figure 16). Vertical pink dashed lines indicate the 24-hour period of 13 June 2020 in each of the forecasts.

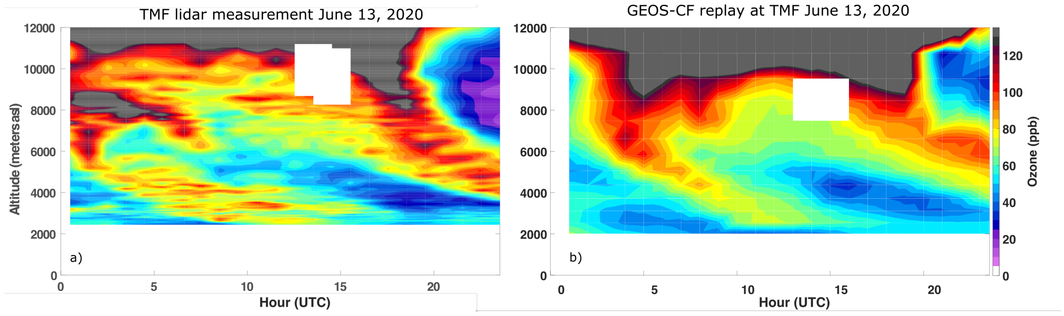

Figure 16. O_3 curtains on 13 June 2020 from a) the TMTOL measurements (30 m vertical resolution) and b) similar to Figure 15 except GEOS-CF replay O_3 for the hours of TMTOL operation. The white areas are where high quality lidar data was unavailable. For comparison, the co-located model data are also removed and indicated as white space.

the stratosphere. Specifically, for surface air quality, it is important that GEOS-CF simulates the stratosphere to troposphere transport as stratospheric O_3 can be transported to the surface and impact surface air quality. Based on this new capability from the GEOS forecast models, GEOS-CF is used in a daily tailored email alert systems for the TOLNet operators. Furthermore, with the meteorology and composition on an identical grid, this makes it ideal to support satellite observations that need a priori information from a model for the trace gas retrievals or to diagnose stratospheric from tropospheric air masses. Instrument teams, such as for TEMPO (Tropospheric Emissions: Monitoring of Pollution; Zoogman et al., 2017), will benefit from near-real time prior information provided by GEOS-CF for their satellite retrievals.

This study focused on concentrations of stratospheric O_3 and chemical species which play a role directly or indirectly in stratospheric O_3 chemistry. Not all chemical species simulated by GEOS-CF have observations available for validation, however an extensive list of chemical species on 3D model output are made available to the public for research purposes (Knowland et al., 2020). Comparisons against independent observations focused on the year 2020, allowing several months for the stratosphere to stabilize after updates were made to the GEOS-Chem UCX module on 31 July 2019 for improved stratospheric chemistry and composition in the GEOS-CF product. Observation suite included ozonesondes and satellites (namely ACE-FTS, MLS, and SAGE III/ISS) to provide a general overview of the global state of the GEOS-CF stratospheric composition. Since the GEOS-CF replay O_3 is constrained by observations by nudging towards the GEOS FP assimilated O_3 product, it is expected to agree well with independent observations in the stratosphere. The median O_3 simulated in GEOS-CF colocated with 20 ozonesonde locations agrees well in the stratosphere (400 to 10 hPa), and the median percent bias is within $\pm$ 20 % through most of the stratosphere. GEOS-CF correlates well with SAGE III/ISS observations ($r > 0.92$) between 100 and 4.6 hPa, but near the stratopause the relationships tend to break down ($r = 0.61$ at 1 hPa). Overall, the spatial patterns of the GEOS-CF simulated concentrations agree well with MLS and ACE-FTS for chlorine (HCl and ClO) and nitrogen (HNO_3; ACE-FTS only for N_2O, NO_x*, and NO_y) species.

With the inclusion of the complex chemistry in GEOS-CF, during extremely low column O_3 events, such as occurred within the NH and SH polar vortexes of 2020, the GEOS-CF forecasts can realistically predict key features of stratospheric O_3 variability. GEOS-CF captures the dynamical and chemical environments of the polar vortexes since heterogeneous reactions on PSCs are represented in the GEOS-Chem UCX mechanism. Specifically, it simulates low concentrations of HCl within the polar vortex and high concentrations of ClO within the sunlit portion, which leads to the destruction of O_3 within the vortex. While biases can exist in the initial conditions and forecasts, in situations where the bias is unimportant or can be corrected, GEOS-CF forecasts should prove especially useful. Future development, as more years of GEOS-CF output become available, will focus on better characterizing this bias. There is also the potential for longer, 10-day, O_3 forecasts pending future demand.

One new development from GMAO is the expanded GEOS DAS to multi-constituent assimilation ("CoDAS"). Demonstrated by Wargan, Weir, et al. (2020), the assimilation of stratospheric O_3, HCl, H_2O, and N_2O from MLS with a stratospheric chemistry model can offer a more realistic representation of important species related to stratospheric O_3 recovery, in particular within the polar vortex. Stratospheric H_2O in reanalysis products are historically poor (Davis et al., 2020), and without an observational constraint on H_2O above the tropopause, the GEOS-CF stratospheric water vapor is also biased compared to independent observations from MLS and ACE-FTS (Figure S5). In addition to HNO_3, water vapor is important for PSCs and other heterogeneous processes. Future developments for the GEOS-CF system include incorporating the CoDAS system to constrain both tropospheric and stratospheric constituents. The first test will include the assimilation of stratospheric O_3 to remove the need for the O_3 nudging technique. With the assimilation of satellite-retrieved H_2O and other stratospheric species, GEOS-CF would likely improve on the spatial distribution of these and other related chemical species globally, and especially in and around a polar vortex.

Acknowledgments

All GEOS-CF model output is centrally stored at the NASA Center for Climate Simulation (NCCS). Public access to these archives is provided by the GMAO at `https://gmao.gsfc.nasa.gov/weather_prediction/GEOS-CF/data_access` through model output access tools including OPeNDAP and Hypertext Transfer Protocol (HTTP). The SBUV merged dataset is available from `https://acd-ext.gsfc.nasa.gov/Data_services/merged/index.html`, OMI "TOMS-like" level 3 gridded product (Bhartia, 2012) available from `https://disc.gsfc.nasa.gov/datasets/OMTO3d_003/summary`, SAGE III-ISS data is available from the NASA Langley Research Center Atmospheric Sciences Data center (`https://eosweb.larc.nasa.gov/project/SAGE\%20III-ISS`), OMI and MLS data is available at `https://disc.gsfc.nasa.gov/`, and TOLNet available from `https://www-air.larc.nasa.gov/missions/TOLNet/data.html`. The ozonesondes are available from `http://www.woudc.org` and `ftp://aftp.cmdl.noaa.gov/data/ozwv/ozonesonde/`. ACE-FTS measurements are available, following registration, from `http://www.ace.uwaterloo.ca/`, with the data quality information available at `https://dataverse.scholarsportal.info/dataset.xhtml?persistentId=doi:10.5683/SP2/BC4ATC`.

Resources supporting the GEOS-CF and GEOS CCM model simulations were provided by the NCCS. KEK, CAK, PAW, KW, LC, LO, SP acknowledge support by the NASA Modeling, Analysis and Prediction (MAP) Program (Project manager David Considine). Support for EF, JL, QL was provided by the CCM work package funded by the NASA MAP. MJ was funded for this work by the NASA Tropospheric Composition Program as part of the TOLNet Science Team. The research carried out at the Jet Propulsion Laboratory, California Institute of Technology, was performed under a contract with the National Aeronautics and Space Administration (80NM0018D0004). The Atmospheric Chemistry Experiment is a Canadian-led mission mainly supported by the CSA.

References

Bak, J., Liu, X., Kim, J.-H., Haffner, D. P., Chance, K., Yang, K., & Sun, K. (2017). Characterization and correction of OMPS nadir mapper measurements for ozone profile retrievals. *Atmospheric Measurement Techniques*, *10*(11), 4373–4388. Retrieved from `https://amt.copernicus.org/articles/10/4373/`

2017/ doi: 10.5194/amt-10-4373-2017
Bernath, P. F. (2017). The Atmospheric Chemistry Experiment (ACE). *J. Quant. Spectrosc. Ra.*, *186*(Supplement C), 3 - 16. (Satellite Remote Sensing and Spectroscopy: Joint ACE-Odin Meeting, October 2015) doi: 10.1016/j.jqsrt.2016.04.006
Bernath, P. F., McElroy, C. T., Abrams, M. C., Boone, C. D., Butler, M., Camy-Peyret, C., ... Zou, J. (2005). Atmospheric Chemistry Experiment (ACE): Mission overview. *Geophys. Res. Lett.*, *32*(15). (L15S01) doi: 10.1029/2005GL022386
Bey, I., Jacob, D. J., Yantosca, R. M., Logan, J. A., Field, B. D., Fiore, A. M., ... Schultz, M. G. (2001). Global modeling of tropospheric chemistry with assimilated meteorology: Model description and evaluation. *Journal of Geophysical Research: Atmospheres*, *106*(D19), 23073-23095. doi: 10.1029/2001JD000807
Bhartia, P. K. (2012). OMI/Aura TOMS-Like Ozone, Aerosol Index, Cloud Radiance Fraction L3 1 day 1 degree x 1 degree V3, NASA Goddard Space Flight Center, Goddard Earth Sciences Data and Information Services Center (GES DISC), Accessed: June 2020 and January 2021.
doi: 10.5067/Aura/OMI/DATA3001
Bhartia, P. K., & McPeters, R. D. (2018). The discovery of the Antarctic Ozone Hole. *Comptes Rendus Geoscience*, *350*(7), 335-340. doi: 10.1016/j.crte.2018.04.006
Boone, C. D., Bernath, P. F., Cok, D., Jones, S. C., & Steffen, J. (2020). Version 4 retrievals for the atmospheric chemistry experiment Fourier transform spectrometer (ACE-FTS) and imagers. *Journal of Quantitative Spectroscopy and Radiative Transfer*, *247*, 106939. Retrieved from https://www.sciencedirect.com/science/article/pii/S0022407319305916 doi: https://doi.org/10.1016/j.jqsrt.2020.106939
Brasseur, G. P., & Solomon, S. (2005). *Aeronomy of the middle atmosphere: Chemistry and physics of the stratosphere and mesosphere* (Vol. 32). Springer Science & Business Media.
Bucsela, E. J., Krotkov, N. A., Celarier, E. A., Lamsal, L. N., Swartz, W. H., Bhartia, P. K., ... Pickering, K. E. (2013). A new stratospheric and tropospheric NO_2 retrieval algorithm for nadir-viewing satellite instruments: applications to OMI. *Atmospheric Measurement Techniques*, *6*(10), 2607–2626. Retrieved from https://amt.copernicus.org/articles/6/2607/2013/ doi: 10.5194/amt-6-2607-2013
Burkholder, J. B., Sander, S. P., Abbatt, J. P. D., Barker, J. R., Huie, R. E., Kolb, C. E., ... Wine, P. H. (2015). Chemical Kinetics and Photochemical Data for Use in Atmospheric Studies, Evaluation No. 18, JPL Publication 15-10. *Jet Propulsion Laboratory, Pasadena, CA.* Retrieved from http://jpldataeval.jpl.nasa.gov
Carpenter, L. J., & Daniel, J. S. (2018). Scenarios and information for policymakers, chapter 6 in scientific assessment of ozone depletion: 2018. *Global Ozone Research and Monitoring Project — Report No. 58.* Retrieved from https://csl.noaa.gov/assessments/ozone/2018/downloads/Chapter6_2018OzoneAssessment.pdf
Chang, A. Y., Salawitch, R. J., Michelsen, H. A., Gunson, M. R., Abrams, M. C., Zander, R., ... Stiller, G. P. (1996). A comparison of measurements from ATMOS and instruments aboard the ER-2 aircraft: Tracers of atmospheric transport. *Geophysical Research Letters*, *23*(17), 2389-2392. doi: 10.1029/96GL01677
Chen, Q., Schmidt, J. A., Shah, V., Jaeglé, L., Sherwen, T., & Alexander, B. (2017). Sulfate production by reactive bromine: Implications for the global sulfur and reactive bromine budgets. *Geophysical Research Letters*, *44*(13), 7069-7078. doi: https://doi.org/10.1002/2017GL073812

Chouza, F., Leblanc, T., Brewer, M., & Wang, P. (2019). Upgrade and automation of the JPL Table Mountain Facility tropospheric ozone lidar (TMTOL) for near-ground ozone profiling and satellite validation. *Atmospheric Measurement Techniques*, *12*(1), 569–583. Retrieved from https://amt.copernicus.org/articles/12/569/2019/ doi: 10.5194/amt-12-569-2019

Cisewski, M., Zawodny, J., Gasbarre, J., Eckman, R., Topiwala, O., Nandkishoreand Rodriguez-Alvarez, Cheek, D., & Hall, S. (2014). The Stratospheric Aerosol and Gas Experiment (SAGE III) on the International Space Station (ISS) Mission. *Proc. SPIE*, *9241*. (Sensors, Systems, and Next-Generation Satellites XVIII, 924107 (11 November 2014)) doi: 10.1117/12.2073131

Clark, H., Bennouna, Y., Tsivlidou, M., Wolff, P., Sauvage, B., Barret, B., ... Thouret, V. (2021). The effects of the covid-19 lockdowns on the composition of the troposphere as seen by iagos. *Atmospheric Chemistry and Physics Discussions*, *2021*, 1–33. doi: 10.5194/acp-2021-479

Collins, M., Knutti, R., Arblaster, J., Dufresne, J.-L., Fichefet, T., Friedlingstein, P., ... others (2013). Long-term climate change: projections, commitments and irreversibility. In *Climate Change 2013-The Physical Science Basis: Contribution of Working Group I to the Fifth Assessment Report of the Intergovernmental Panel on Climate Change* (pp. 1029–1136). Cambridge University Press.

Crutzen, P. J. (1970). The influence of nitrogen oxides on the atmospheric ozone content. *Quarterly Journal of the Royal Meteorological Society*, *96*(408), 320-325. doi: 10.1002/qj.49709640815

Dacic, N., Sullivan, J. T., Knowland, K. E., Wolfe, G. M., Oman, L. D., Berkoff, T. A., & Gronoff, G. P. (2020). Evaluation of NASA's high-resolution global composition simulations: Understanding a pollution event in the Chesapeake Bay during the summer 2017 OWLETS campaign. *Atmospheric Environment*, *222*, 117133. doi: 10.1016/j.atmosenv.2019.117133

Damadeo, R. P., Zawodny, J. M., Remsberg, E. E., & Walker, K. A. (2018). The impact of nonuniform sampling on stratospheric ozone trends derived from occultation instruments. *Atmos. Chem. Phys.*, *18*(2), 535–554. Retrieved from https://acp.copernicus.org/articles/18/535/2018/ doi: 10.5194/acp-18-535-2018

Dameris, M., Loyola, D. G., Nützel, M., Coldewey-Egbers, M., Lerot, C., Romahn, F., & van Roozendael, M. (2021). Record low ozone values over the Arctic in boreal spring 2020. *Atmos. Chem. Phys.*, *21*(2), 617–633. doi: 10.5194/acp-21-617-2021

Darmenov, A., & da Silva, A. (2015). *The Quick Fire Emissions Dataset (QFED): Documentation of versions 2.1, 2.2 and 2.4* (Tech. Rep.). NASA/TM–2015–104606, Vol. 38.

Davis, S. M., Damadeo, R., Flittner, D. E., Rosenlof, K. H., Park, M., Randel, W. J., ... Vomel, H. (2020). Validation of sage iii/iss solar water vapor data with correlative satellite and balloon-borne measurements. *Earth and Space Science Open Archive*, 25. doi: 10.1002/essoar.10504226.1

DeLand, M. T., Bhartia, P. K., Kramarova, N., & Chen, Z. (2020). OMPS LP Observations of PSC Variability During the NH 2019–2020 Season. *Geophysical Research Letters*, *47*(20), e2020GL090216. (e2020GL090216 2020GL090216) doi: 10.1029/2020GL090216

Douglass, A. R., Prather, M. J., Hall, T. M., Strahan, S. E., Rasch, P. J., Sparling, L. C., ... Rodriguez, J. M. (1999). Choosing meteorological input for the global modeling initiative assessment of high-speed aircraft. *Journal of Geophysical Research: Atmospheres*, *104*(D22), 27545-27564. doi: 10.1029/1999JD900827

Douglass, A. R., Stolarski, R. S., Strahan, S. E., & Connell, P. S. (2004). Radicals and reservoirs in the GMI chemistry and transport model: Comparison to measurements. *Journal of Geophysical Research: Atmospheres*, *109*(D16). doi: 10.1029/2004JD004632

Duncan, B. N., Malings, C. A., Knowland, K. E., Anderson, D. C., Prados, A. I., Keller, C. A., ... Ensz, H. (2021). Augmenting the standard operating procedures of health and air quality stakeholders with nasa resources. *GeoHealth*, *5*(9), e2021GH000451. doi: 10.1029/2021GH000451

Duncan, B. N., Strahan, S. E., Yoshida, Y., Steenrod, S. D., & Livesey, N. (2007). Model study of the cross-tropopause transport of biomass burning pollution. *Atmospheric Chemistry and Physics*, *7*(14), 3713–3736. Retrieved from `https://acp.copernicus.org/articles/7/3713/2007/` doi: 10.5194/acp-7-3713-2007

Dupuy, E., Walker, K. A., Kar, J., Boone, C. D., McElroy, C. T., Bernath, P. F., ... Zawodny, J. M. (2009). Validation of ozone measurements from the Atmospheric Chemistry Experiment (ACE). *Atmos. Chem. Phys.*, *9*(2), 287–343. doi: 10.5194/acp-9-287-2009

Eastham, S. D., Weisenstein, D. K., & Barrett, S. R. (2014). Development and evaluation of the unified tropospheric–stratospheric chemistry extension (UCX) for the global chemistry-transport model GEOS-Chem. *Atmospheric Environment*, *89*, 52 - 63. doi: 10.1016/j.atmosenv.2014.02.001

Engel, A., & Rigby, M. (2018). Update on Ozone-Depleting Substances (ODSs) and Other Gases of Interest to the Montreal Protocol, Chapter 1 in Scientific Assessment of Ozone Depletion: 2018. *Global Ozone Research and Monitoring Project — Report No. 58*. Retrieved from `https://csl.noaa.gov/assessments/ozone/2018/downloads/Chapter1_2018OzoneAssessment.pdf`

Errera, Q., Chabrillat, S., Christophe, Y., Debosscher, J., Hubert, D., Lahoz, W., ... Walker, K. (2019). Technical note: Reanalysis of Aura MLS chemical observations. *Atmos. Chem. Phys.*, *19*(21), 13647–13679. Retrieved from `https://acp.copernicus.org/articles/19/13647/2019/` doi: 10.5194/acp-19-13647-2019

Farman, J. C., Gardiner, B. G., & Shanklin, J. D. (1985, May). Large losses of total ozone in Antarctica reveal seasonal ClOx/NOx interaction. *Nature*, *315*(6016), 207–210. Retrieved from `https://doi.org/10.1038/315207a0` doi: 10.1038/315207a0

Feng, W., Dhomse, S. S., Arosio, C., Weber, M., Burrows, J. P., Santee, M. L., & Chipperfield, M. P. (2021). Arctic Ozone Depletion in 2019/20: Roles of Chemistry, Dynamics and the Montreal Protocol. *Geophys. Res. Lett.*, *48*(4), e2020GL091911. doi: 10.1029/2020GL091911

Frith, S. M., Kramarova, N. A., Stolarski, R. S., McPeters, R. D., Bhartia, P. K., & Labow, G. J. (2014). Recent changes in total column ozone based on the SBUV Version 8.6 Merged Ozone Data Set. *J. Geophys. Res.*, *119*(16), 9735-9751. doi: https://doi.org/10.1002/2014JD021889

Funke, B., López-Puertas, M., Gil-López, S., von Clarmann, T., Stiller, G. P., Fischer, H., & Kellmann, S. (2005). Downward transport of upper atmospheric NOx into the polar stratosphere and lower mesosphere during the Antarctic 2003 and Arctic 2002/2003 winters. *Journal of Geophysical Research: Atmospheres*, *110*(D24). doi: 10.1029/2005JD006463

Gronoff, G., Berkoff, T., Knowland, K., Lei, L., Shook, M., Fabbri, B., ... Langford, A. (2021). Case study of stratospheric Intrusion above Hampton, Virginia: lidar-observation and modeling analysis. *Atmospheric Environment*, 118498. Retrieved from `https://www.sciencedirect.com/science/article/pii/S1352231021003198` doi: https://doi.org/10.1016/j.atmosenv.2021.118498

Grooß, J.-U., Müller, R., Spang, R., Tritscher, I., Wegner, T., Chipperfield, M. P., ... Madronich, S. (2018). On the discrepancy of HCl processing in the core of the wintertime polar vortices. *Atmos. Chem. Phys.*, *18*(12), 8647–8666. doi: 10.5194/acp-18-8647-2018

Hanson, D. R., & Ravishankara, A. R. (1992). Heterogeneous chemistry of hydrogen bromide and hydrogen fluoride. *J. Phys. Chem.*, *96*(23), 9441-9446. doi: 10.1021/j100202a069

Hanson, D. R., & Ravishankara, A. R. (1995). Heterogeneous chemistry of bromine species in sulfuric acid under stratospheric conditions. *Geophys. Res. Lett.*, *22*(4), 385-388. doi: 10.1029/94GL03379

Holton, J. R. (1986). A dynamically based transport parameterization for one-dimensional photochemical models of the stratosphere. *Journal of Geophysical Research: Atmospheres*, *91*(D2), 2681-2686. doi: 10.1029/JD091iD02p02681

Hu, L., Keller, C. A., Long, M. S., Sherwen, T., Auer, B., Da Silva, A., ... Jacob, D. J. (2018). Global simulation of tropospheric chemistry at 12.5 km resolution: performance and evaluation of the GEOS-Chem chemical module (v10-1) within the NASA GEOS Earth system model (GEOS-5 ESM). *Geoscientific Model Development*, *11*(11), 4603–4620. Retrieved from https://gmd.copernicus.org/articles/11/4603/2018/ doi: 10.5194/gmd-11-4603-2018

Inness, A., Chabrillat, S., Flemming, J., Huijnen, V., Langenrock, B., Nicolas, J., ... Razinger, M. (2020). Exceptionally Low Arctic Stratospheric Ozone in Spring 2020 as Seen in the CAMS Reanalysis. *Journal of Geophysical Research: Atmospheres*, *125*(23), e2020JD033563. doi: 10.1029/2020JD033563

Jin, J. J., Semeniuk, K., Beagley, S. R., Fomichev, V. I., Jonsson, A. I., McConnell, J. C., ... Dupuy, E. (2009). Comparison of CMAM simulations of carbon monoxide (CO), nitrous oxide (N_2O), and methane (CH_4) with observations from Odin/SMR, ACE-FTS, and Aura/MLS. *Atmospheric Chemistry and Physics*, *9*(10), 3233–3252. doi: 10.5194/acp-9-3233-2009

Johnson, M. S., Strawbridge, K., Knowland, K. E., Keller, C., & Travis, M. (2021). Long-range transport of Siberian biomass burning emissions to North America during FIREX-AQ. *Atmos. Environ.*, *252*, 118241. Retrieved from https://www.sciencedirect.com/science/article/pii/S1352231021000595 doi: https://doi.org/10.1016/j.atmosenv.2021.118241

Keene, W. C., Khalil, M. A. K., Erickson III, D. J., McCulloch, A., Graedel, T. E., Lobert, J. M., ... Li, Y. F. (1999). Composite global emissions of reactive chlorine from anthropogenic and natural sources: Reactive Chlorine Emissions Inventory. *J. Geophys. Res.*, *104*(D7), 8429-8440. doi: https://doi.org/10.1029/1998JD100084

Keller, C. A., Knowland, K. E., Duncan, B. N., Liu, J., Anderson, D. C., Das, S., ... Pawson, S. (2021). Description of the NASA GEOS Composition Forecast Modeling System GEOS-CF v1.0. *Journal of Advances in Modeling Earth Systems*, *13*(4), e2020MS002413. doi: 10.1029/2020MS002413

Keller, C. A., Long, M. S., Yantosca, R. M., Da Silva, A. M., Pawson, S., & Jacob, D. J. (2014). HEMCO v1.0: a versatile, ESMF-compliant component for calculating emissions in atmospheric models. *Geosci. Model Dev.*, *7*(4), 1409–1417. Retrieved from https://gmd.copernicus.org/articles/7/1409/2014/ doi: 10.5194/gmd-7-1409-2014

Kinnison, D. E., Connell, P. S., Rodriguez, J. M., Rotman, D. A., Considine, D. B., Tannahill, J., ... Prather, M. J. (2001). The global modeling initiative assessment model: Application to high-speed civil transport perturbation. *Journal of Geophysical Research: Atmospheres*, *106*(D2), 1693-1711. doi: 10.1029/2000JD900406

Knowland, K. E., Keller, C. A., & Lucchesi, R. (2020). File Specification for GEOS-CF Products, GMAO Office Note No. 17 (Version 1.1) 37 pp. *Available at: http://gmao.gsfc.nasa.gov/pubs/office_notes.php.*

Knowland, K. E., Ott, L. E., Duncan, B. N., & Wargan, K. (2017). Stratospheric Intrusion-Influenced Ozone Air Quality Exceedances Investigated in the NASA MERRA-2 Reanalysis. *Geophys. Res. Lett.*. (2017GL074532) doi:

10.1002/2017GL074532

Koike, M., Kondo, Y., Takegawa, N., Lefevre, F., Ikeda, H., Irie, H., ... Masui, Y. (2002). Redistribution of reactive nitrogen in the Arctic lower stratosphere in the 1999/2000 winter. *Journal of Geophysical Research: Atmospheres*, *107*(D20), SOL 17-1-SOL 17-16. doi: 10.1029/2001JD001089

Krzyzanowski, M., & Cohen, A. (2008). Update of WHO air quality guidelines. *Air Qual. Atmos. Health*, *1*, 7–13. doi: 10.1007/s11869-008-0008-9

Kuang, S., Newchurch, M. J., Burris, J., Wang, L., Knupp, K., & Huang, G. (2012). Stratosphere-to-troposphere transport revealed by ground-based lidar and ozonesonde at a midlatitude site. *Journal of Geophysical Research: Atmospheres*, *117*(D18). doi: 10.1029/2012JD017695

Kuang, S., Newchurch, M. J., Johnson, M. S., Wang, L., Burris, J., Pierce, R. B., ... Feng, N. (2017). Summertime tropospheric ozone enhancement associated with a cold front passage due to stratosphere-to-troposphere transport and biomass burning: Simultaneous ground-based lidar and airborne measurements. *J. Geophys. Res.*, *122*(2), 1293–1311. (2016JD026078) doi: 10.1002/2016JD026078

Langford, A. O., Aikin, K. C., Eubank, C. S., & Williams, E. J. (2009). Stratospheric contribution to high surface ozone in Colorado during springtime. *Geophys. Res. Lett.*, *36*(12). Retrieved from http://dx.doi.org/10.1029/2009GL038367 (L12801) doi: 10.1029/2009GL038367

Lawrence, Z. D., Perlwitz, J., Butler, A. H., Manney, G. L., Newman, P. A., Lee, S. H., & Nash, E. R. (2020). The Remarkably Strong Arctic Stratospheric Polar Vortex of Winter 2020: Links to Record-Breaking Arctic Oscillation and Ozone Loss. *J. Geophys. Res.*, *125*(22), e2020JD033271. (e2020JD033271 10.1029/2020JD033271) doi: 10.1029/2020JD033271

Leblanc, T., Brewer, M. A., Wang, P. S., Granados-Muñoz, M. J., Strawbridge, K. B., Travis, M., ... Newchurch, M. J. (2018). Validation of the TOLNet lidars: the Southern California Ozone Observation Project (SCOOP). *Atmospheric Measurement Techniques*, *11*(11), 6137–6162. Retrieved from https://amt.copernicus.org/articles/11/6137/2018/ doi: 10.5194/amt-11-6137-2018

Lecouffe, A., Godin-Beekmann, S., Pazmiño, A., & Hauchecorne, A. (2021). Evolution of the stratospheric polar vortex edge intensity and duration in the Southern hemisphere over the 1979–2020 period. *Atmospheric Chemistry and Physics Discussions*, *2021*, 1–23. doi: 10.5194/acp-2021-676

Le Quéré, C., Jackson, R. B., Jones, M. W., Smith, A. J. P., Abernethy, S., Andrew, R. M., ... Peters, G. P. (2020, July). Temporary reduction in daily global CO2 emissions during the COVID-19 forced confinement. *Nature Climate Change*, *10*(7), 647–653. doi: 10.1038/s41558-020-0797-x

Levelt, P. F., Joiner, J., Tamminen, J., Veefkind, J. P., Bhartia, P. K., Stein Zweers, D. C., ... Wargan, K. (2018). The ozone monitoring instrument: overview of 14 years in space. *Atmos. Chem. Phys.*, *18*(8), 5699–5745. Retrieved from https://acp.copernicus.org/articles/18/5699/2018/ doi: 10.5194/acp-18-5699-2018

Levelt, P. F., van den Oord, G. H. J., Dobber, M. R., Malkki, A., Visser, H., de Vries, J., ... Saari, H. (2006, May). The ozone monitoring instrument. *IEEE Trans. Geosci. Remote Sens.*, *44*(5), 1093-1101. doi: 10.1109/TGRS.2006.872333

Livesey, N. J., Read, W. G., Froidevaux, L., Lambert, A., Santee, M. L., Schwartz, M. J., ... Nedoluha, G. E. (2021). Investigation and amelioration of long-term instrumental drifts in water vapor and nitrous oxide measurements from the Aura Microwave Limb Sounder (MLS) and their implications for studies of variability and trends. *Atmospheric Chemistry and Physics Discussions*, *2021*, 1–32. doi: 10.5194/acp-2021-440

Livesey, N. J., Read, W. G., Wagner, P. A., Froidevaux, L., Santee, M. L., Schwartz, M. J., ... Lay, R. R. (2020). Version 5.0x Level 2 and 3 data quality and description document, JPL D-105336 Rev. A. *Retrieved from https://mls.jpl.nasa.gov/data/v5-0_data_quality_document.pdf*.

Long, M. S., Yantosca, R., Nielsen, J. E., Keller, C. A., da Silva, A., Sulprizio, M. P., ... Jacob, D. J. (2015). Development of a grid-independent GEOS-Chem chemical transport model (v9-02) as an atmospheric chemistry module for Earth system models. *Geosci. Model Dev.*, *8*(3), 595–602. Retrieved from `https://www.geosci-model-dev.net/8/595/2015/` doi: 10.5194/gmd-8-595-2015

Lucchesi, R. (2015). File specification for GEOS-5 FP-IT, GMAO Office Note No. 2 (Version 1.4). *Available at: http://gmao.gsfc.nasa.gov/pubs/office_notes.php*.

Lucchesi, R. (2018). File specification for GEOS FP, GMAO Office Note No. 4 (Version 1.2). *Available at: http://gmao.gsfc.nasa.gov/pubs/office_notes.php*, 61pp.

Mahlman, J. D., Levy II, H., & Moxim, W. J. (1986). Three-dimensional simulations of stratospheric N2O: Predictions for other trace constituents. *Journal of Geophysical Research: Atmospheres*, *91*(D2), 2687-2707. doi: 10.1029/JD091iD02p02687

Manney, G. L., Harwood, R. S., MacKenzie, I. A., Minschwaner, K., Allen, D. R., Santee, M. L., ... Fuller, R. A. (2009). Satellite observations and modeling of transport in the upper troposphere through the lower mesosphere during the 2006 major stratospheric sudden warming. *Atmospheric Chemistry and Physics*, *9*(14), 4775–4795. doi: 10.5194/acp-9-4775-2009

Manney, G. L., Livesey, N. J., Santee, M. L., Froidevaux, L., Lambert, A., Lawrence, Z. D., ... Fuller, R. A. (2020). Record-Low Arctic Stratospheric Ozone in 2020: MLS Observations of Chemical Processes and Comparisons With Previous Extreme Winters. *Geophys. Res. Lett.*, *47*(16), e2020GL089063. doi: 10.1029/2020GL089063

Mauldin, L. E., Salikhov, R., Habib, S., Vladimirov, A. G., Carraway, D., Petrenko, G., & Comella, J. (1998). Meteor-3M(1)/Stratospheric Aerosol and Gas Experiment III (SAGE III) jointly sponsored by the National Aeronautics and Space Administration and the Russian Space Agency. *Proc. SPIE*, *3501*. ((18 August 1998)) doi: 10.1117/12.317767

McCormick, M. P., & Chu, W. P. (2004). *Stratospheric Aerosol and Gas Experiment III (SAGE III): Data Product User's Guide.* Version 1.5, July 2004, National Aeronautics and Space Administration.

McCormick, M. P., Lei, L., Hill, M. T., Anderson, J., Querel, R., & Steinbrecht, W. (2020). Early results and validation of SAGE III-ISS ozone profile measurements from onboard the International Space Station. *Atmos. Meas. Tech.*, *13*(3), 1287–1297. Retrieved from `https://amt.copernicus.org/articles/13/1287/2020/` doi: 10.5194/amt-13-1287-2020

McDermid, I. S., Beyerle, G., Haner, D. A., & Leblanc, T. (2002, Dec). Redesign and improved performance of the tropospheric ozone lidar at the Jet Propulsion Laboratory Table Mountain Facility. *Appl. Opt.*, *41*(36), 7550–7555. doi: 10.1364/AO.41.007550

McPeters, R., Kroon, M., Labow, G., Brinksma, E., Balis, D., Petropavlovskikh, I., ... Levelt, P. F. (2008). Validation of the Aura Ozone Monitoring Instrument total column ozone product. *J. Geophys. Res.*, *113*(D15). doi: 10.1029/2007JD008802

Molina, M. J., & Rowland, F. S. (1974a). Predicted present stratospheric abundances of chlorine species from photodissociation of carbon tetrachloride. *Geophys. Res. Lett.*, *1*(7), 309-312. doi: https://doi.org/10.1029/GL001i007p00309

Molina, M. J., & Rowland, F. S. (1974b, June). Stratospheric sink for chlorofluoromethanes: chlorine atom-catalysed destruction of ozone. *Nature*, *249*(5460), 810–812. Retrieved from https://doi.org/10.1038/249810a0 doi: 10.1038/249810a0

Molod, A., Takacs, L., Suarez, M., & Bacmeister, J. (2015). Development of the GEOS-5 atmospheric general circulation model: evolution from MERRA to MERRA2. *Geosci. Model Dev.*, *8*(5), 1339–1356. doi: 10.5194/gmd-8-1339-2015

Murray, L. T., Jacob, D. J., Logan, J. A., Hudman, R. C., & Koshak, W. J. (2012). Optimized regional and interannual variability of lightning in a global chemical transport model constrained by LIS/OTD satellite data. *Journal of Geophysical Research: Atmospheres*, *117*(D20). doi: https://doi.org/10.1029/2012JD017934

Nielsen, J. E., Pawson, S., Molod, A., Auer, B., da Silva, A. M., Douglass, A. R., ... Wargan, K. (2017). Chemical Mechanisms and Their Applications in the Goddard Earth Observing System (GEOS) Earth System Model. *Journal of Advances in Modeling Earth Systems*, *9*(8), 3019-3044. doi: 10.1002/2017MS001011

Orbe, C., Oman, L. D., Strahan, S. E., Waugh, D. W., Pawson, S., Takacs, L. L., & Molod, A. M. (2017). Large-Scale Atmospheric Transport in GEOS Replay Simulations. *J. Adv. Model. Earth Syst.*. Retrieved from http://dx.doi.org/10.1002/2017MS001053 doi: 10.1002/2017MS001053

Ott, L. E., Duncan, B. N., Thompson, A. M., Diskin, G., Fasnacht, Z., Langford, A. O., ... Yoshida, Y. (2016). Frequency and impact of summertime stratospheric intrusions over Maryland during DISCOVER-AQ (2011): New evidence from NASA's GEOS-5 simulations. *J. Geophys. Res.*, *121*(7), 3687–3706. doi: 10.1002/2015JD024052

Parrella, J. P., Jacob, D. J., Liang, Q., Zhang, Y., Mickley, L. J., Miller, B., ... Van Roozendael, M. (2012). Tropospheric bromine chemistry: implications for present and pre-industrial ozone and mercury. *Atmospheric Chemistry and Physics*, *12*(15), 6723–6740. Retrieved from https://acp.copernicus.org/articles/12/6723/2012/ doi: 10.5194/acp-12-6723-2012

Plumb, R. A. (2007). Tracer interrelationships in the stratosphere. *Reviews of Geophysics*, *45*(4). doi: 10.1029/2005RG000179

Randall, C. E., Harvey, V. L., Manney, G. L., Orsolini, Y., Codrescu, M., Sioris, C., ... Russell III, J. M. (2005). Stratospheric effects of energetic particle precipitation in 2003–2004. *Geophysical Research Letters*, *32*(5). doi: 10.1029/2004GL022003

Randall, C. E., Harvey, V. L., Singleton, C. S., Bailey, S. M., Bernath, P. F., Codrescu, M., ... Russell III, J. M. (2007). Energetic particle precipitation effects on the Southern Hemisphere stratosphere in 1992–2005. *J. Geophys. Res.*, *112*(D8). doi: 10.1029/2006JD007696

Reimann, S., Elkins, J. W., Fraser, P. J., Hall, B. D., Kurylo, M. J., Mahieu, E., ... Weiss, R. F. (2018). Observing the atmospheric evolution of ozone-depleting substances. *Comptes Rendus Geoscience*, *350*(7), 384-392. (30th Anniversary of the Montreal Protocol: From the safeguard of the ozone layer to the protection of the Earth Climate) doi: 10.1016/j.crte.2018.08.008

Robinson, J., Kotsakis, A., Santos, F., Swap, R., Knowland, K., Labow, G., ... Cede, A. (2020). Using networked Pandora observations to capture spatiotemporal changes in total column ozone associated with stratosphere-to-troposphere transport. *Atmospheric Research*, *238*, 104872. doi: 10.1016/j.atmosres.2020.104872

Rotman, D. A., Tannahill, J. R., Kinnison, D. E., Connell, P. S., Bergmann, D., Proctor, D., ... Kawa, S. R. (2001). Global Modeling Initiative assessment model: Model description, integration, and testing of the transport shell. *J. Geophys. Res.*, *106*(D2), 1669-1691. doi: https://doi.org/10.1029/2000JD900463

Rowland, F. S., Spencer, J. E., & Molina, M. J. (1976). Stratospheric formation and photolysis of chlorine nitrate. *J. Phys. Chem.*, *80*(24), 2711-2713. doi: 10.1021/j100565a019

Ruiz, D. J., Prather, M. J., Strahan, S. E., Thompson, R. L., Froidevaux, L., & Steenrod, S. D. (2021). How Atmospheric Chemistry and Transport Drive Surface Variability of N2O and CFC-11. *Journal of Geophysical Research: Atmospheres*, *126*(8), e2020JD033979. doi: 10.1029/2020JD033979

Salawitch, R. J., Gobbi, G. P., Wofsy, S. C., & McElroy, M. B. (1989). Denitrification in the Antarctic stratosphere. *Nature*, *339*(6225), 525–527.

Sander, S. P., Friedl, R. R., Barker, J. R., Burkholder, J. B., Friedl, R. R., Golden, D. M., … Wine, P. H. (2011). Chemical Kinetics and Photochemical Data for Use in Atmospheric Studies, Evaluation Number 17, JPL Publication 10-6. *Jet Propulsion Laboratory, Pasadena, CA.* Retrieved from `http://jpldataeval.jpl.nasa.gov`

Schlink, U., Herbarth, O., Richter, M., Dorling, S., Nunnari, G., Cawley, G., & Pelikan, E. (2006). Statistical models to assess the health effects and to forecast ground-level ozone. *Environ. Model. Soft.*, *21*(4), 547 - 558. doi: 10.1016/j.envsoft.2004.12.002

Schmidt, J. A., Jacob, D. J., Horowitz, H. M., Hu, L., Sherwen, T., Evans, M. J., … Volkamer, R. (2016). Modeling the observed tropospheric BrO background: Importance of multiphase chemistry and implications for ozone, OH, and mercury. *J. Geophys. Res.*, *121*(19), 11,819-11,835. doi: 10.1002/2015JD024229

Sheese, P. E., Walker, K. A., Boone, C. D., Bernath, P. F., Froidevaux, L., Funke, B., … von Clarmann, T. (2017). ACE-FTS ozone, water vapour, nitrous oxide, nitric acid, and carbon monoxide profile comparisons with MIPAS and MLS. *Journal of Quantitative Spectroscopy and Radiative Transfer*, *186*, 63-80. Retrieved from `https://www.sciencedirect.com/science/article/pii/S002240731630067X` (Satellite Remote Sensing and Spectroscopy: Joint ACE-Odin Meeting, October 2015) doi: 10.1016/j.jqsrt.2016.06.026

Sheese, P. E., Walker, K. A., Boone, C. D., Bourassa, A. E., Degenstein, D. A., Froidevaux, L., … Zou, J. (2021). Assessment of the quality of ACE-FTS stratospheric ozone data. *Atmospheric Measurement Techniques Discussions*, *2021*, 1–27. doi: 10.5194/amt-2021-252

Sherwen, T., Evans, M. J., Carpenter, L. J., Andrews, S. J., Lidster, R. T., Dix, B., … Ordóñez, C. (2016). Iodine's impact on tropospheric oxidants: a global model study in GEOS-Chem. *Atmos. Chem. Phys.*, *16*(2), 1161–1186. doi: 10.5194/acp-16-1161-2016

Sherwen, T., Schmidt, J. A., Evans, M. J., Carpenter, L. J., Großmann, K., Eastham, S. D., … Ordóñez, C. (2016). Global impacts of tropospheric halogens (Cl, Br, I) on oxidants and composition in GEOS-Chem. *Atmos. Chem. Phys.*, *16*(18), 12239–12271. doi: 10.5194/acp-16-12239-2016

Siskind, D. E., Bacmeister, J. T., Summers, M. E., & Russell III, J. M. (1997). Two-dimensional model calculations of nitric oxide transport in the middle atmosphere and comparison with Halogen Occultation Experiment data. *Journal of Geophysical Research: Atmospheres*, *102*(D3), 3527-3545. doi: 10.1029/96JD02970

Solomon, S., Crutzen, P. J., & Roble, R. G. (1982). Photochemical coupling between the thermosphere and the lower atmosphere: 1. Odd nitrogen from 50 to 120 km. *Journal of Geophysical Research: Oceans*, *87*(C9), 7206-7220. doi: 10.1029/JC087iC09p07206

Solomon, S., Garcia, R. R., Rowland, F. S., & Wuebbles, D. J. (1986, June). On the depletion of Antarctic ozone. *Nature*, *321*(6072), 755–758. Retrieved from `https://doi.org/10.1038/321755a0` doi: 10.1038/321755a0

Stauffer, R. M., Thompson, A. M., Kollonige, D. E., Witte, J. C., Tarasick, D. W., Davies, J., … Smit, H. G. J. (2020). A Post-2013 Dropoff in Total Ozone at a Third of Global Ozonesonde Stations: Electrochemical Concentration Cell Instrument Artifacts? *Geophys. Res. Lett.*, *47*(11), e2019GL086791. doi: https://doi.org/10.1029/2019GL086791

Stauffer, R. M., Thompson, A. M., Oman, L. D., & Strahan, S. E. (2019). The Effects of a 1998 Observing System Change on MERRA-2-Based Ozone Profile Simulations. *J. Geophys. Res.*, *124*(13), 7429-7441. doi: 10.1029/2019JD030257

Steinbrecht, W., Kubistin, D., Plass-Dülmer, C., Davies, J., Tarasick, D. W., Gathen, P. v. d., … Cooper, O. R. (2021). COVID-19 Crisis Reduces Free Tropospheric Ozone Across the Northern Hemisphere. *Geophys. Res. Lett.*, *48*(5), e2020GL091987. doi: 10.1029/2020GL091987

Sterling, C. W., Johnson, B. J., Oltmans, S. J., Smit, H. G. J., Jordan, A. F., Cullis, P. D., … Witte, J. C. (2018). Homogenizing and estimating the uncertainty in NOAA's long-term vertical ozone profile records measured with the electrochemical concentration cell ozonesonde. *Atmospheric Measurement Techniques*, *11*(6), 3661–3687. Retrieved from https://amt.copernicus.org/articles/11/3661/2018/ doi: 10.5194/amt-11-3661-2018

Stolarski, R. S., & Cicerone, R. J. (1974). Stratospheric Chlorine: a Possible Sink for Ozone. *Canad. J. Chem.*, *52*(8), 1610-1615. doi: 10.1139/v74-233

Stolarski, R. S., Krueger, A. J., Schoeberl, M. R., McPeters, R. D., Newman, P. A., & Alpert, J. C. (1986, August). Nimbus 7 satellite measurements of the springtime Antarctic ozone decrease. *Nature*, *322*(6082), 808–811. Retrieved from https://doi.org/10.1038/322808a0 doi: 10.1038/322808a0

Strahan, S. E., & Douglass, A. R. (2018). Decline in Antarctic Ozone Depletion and Lower Stratospheric Chlorine Determined From Aura Microwave Limb Sounder Observations. *Geophysical Research Letters*, *45*(1), 382-390. doi: 10.1002/2017GL074830

Strahan, S. E., Duncan, B. N., & Hoor, P. (2007). Observationally derived transport diagnostics for the lowermost stratosphere and their application to the GMI chemistry and transport model. *Atmospheric Chemistry and Physics*, *7*(9), 2435–2445. doi: 10.5194/acp-7-2435-2007

Strode, S. A., Rodriguez, J. M., Logan, J. A., Cooper, O. R., Witte, J. C., Lamsal, L. N., … Strahan, S. E. (2015). Trends and variability in surface ozone over the United States. *J. Geophys. Res.*, *120*(17), 9020–9042. Retrieved from http://dx.doi.org/10.1002/2014JD022784 (2014JD022784) doi: 10.1002/2014JD022784

Thompson, A. M., Witte, J. C., Sterling, C., Jordan, A., Johnson, B. J., Oltmans, S. J., … Thiongo, K. (2017). First Reprocessing of Southern Hemisphere Additional Ozonesondes (SHADOZ) Ozone Profiles (1998–2016): 2. Comparisons With Satellites and Ground-Based Instruments. *Journal of Geophysical Research: Atmospheres*, *122*(23), 13,000-13,025. doi: 10.1002/2017JD027406

Toon, O. B., Turco, R. P., & Hamill, P. (1990). Denitrification mechanisms in the polar stratospheres. *Geophysical Research Letters*, *17*(4), 445-448. Retrieved from https://agupubs.onlinelibrary.wiley.com/doi/abs/10.1029/GL017i004p00445 doi: 10.1029/GL017i004p00445

Turner, E. C., Manners, J., Morcrette, C. J., O'Hagan, J. B., & Smedley, A. R. D. (2017). Toward a New UV Index Diagnostic in the Met Office's Forecast Model. *Journal of Advances in Modeling Earth Systems*, *9*(7), 2654-2671. doi: 10.1002/2017MS001050

Wang, H. J. R., Damadeo, R., Flittner, D., Kramarova, N., Taha, G., Davis, S., … Hall, E. (2020). Validation of SAGE III/ISS Solar Occultation Ozone Products With Correlative Satellite and Ground-Based Measurements. *J. Geophys. Res.*, *125*(11), e2020JD032430. (e2020JD032430 2020JD032430) doi: 10.1029/2020JD032430

Wang, L., Newchurch, M. J., Alvarez II, R. J., Berkoff, T. A., Brown, S. S., Carrion, W., ... Weinheimer, A. J. (2017). Quantifying TOLNet ozone lidar accuracy during the 2014 DISCOVER-AQ and FRAPPÉ campaigns. *Atmospheric Measurement Techniques*, *10*(10), 3865–3876. Retrieved from https://amt.copernicus.org/articles/10/3865/2017/ doi: 10.5194/amt-10-3865-2017

Wargan, K., Kramarova, N., Weir, B., Pawson, S., & Davis, S. M. (2020). Toward a Reanalysis of Stratospheric Ozone for Trend Studies: Assimilation of the Aura Microwave Limb Sounder and Ozone Mapping and Profiler Suite Limb Profiler Data. *Journal of Geophysical Research: Atmospheres*, *125*(4), e2019JD031892. doi: 10.1029/2019JD031892

Wargan, K., Labow, G., Frith, S., Pawson, S., Livesey, N., & Partyka, G. (2017). Evaluation of the Ozone Fields in NASA's MERRA-2 Reanalysis. *J. Climate*, *30*(8). Retrieved from http://dx.doi.org/10.1175/JCLI-D-16-0699.1 doi: 10.1175/JCLI-D-16-0699.1

Wargan, K., Orbe, C., Pawson, S., Ziemke, J. R., Oman, L. D., Olsen, M. A., ... Knowland, K. E. (2018). Recent Decline in Extratropical Lower Stratospheric Ozone Attributed to Circulation Changes. *Geophys. Res. Lett.*, *45*(10), 5166-5176. Retrieved from https://agupubs.onlinelibrary.wiley.com/doi/abs/10.1029/2018GL077406 doi: 10.1029/2018GL077406

Wargan, K., Pawson, S., Olsen, M. A., Witte, J. C., Douglass, A. R., Ziemke, J. R., ... Nielsen, J. E. (2015). The global structure of upper troposphere-lower stratosphere ozone in GEOS-5: A multiyear assimilation of EOS Aura data. *J. Geophys. Res.*, *120*(5), 2013–2036. (2014JD022493) doi: 10.1002/2014JD022493

Wargan, K., Weir, B., Manney, G. L., Cohn, S. E., & Livesey, N. J. (2020). The Anomalous 2019 Antarctic Ozone Hole in the GEOS Constituent Data Assimilation System With MLS Observations. *Journal of Geophysical Research: Atmospheres*, *125*(18), e2020JD033335. doi: 10.1029/2020JD033335

Waters, J. W., Froidevaux, L., Harwood, R. S., Jarnot, R. F., Pickett, H. M., Read, W. G., ... Walch, M. J. (2006, May). The Earth Observing System Microwave Limb Sounder (EOS MLS) on the Aura Satellite. *IEEE Trans. Geosci. Remote Sens.*, *44*(5), 1075–1092.

Wetzel, G., Oelhaf, H., Ruhnke, R., Friedl-Vallon, F., Kleinert, A., Kouker, W., ... Fischer, H. (2002). NO_y partitioning and budget and its correlation with N_2O in the Arctic vortex and in summer midlatitudes in 1997. *Journal of Geophysical Research: Atmospheres*, *107*(D16), ACH 3-1-ACH 3-10. doi: 10.1029/2001JD000916

Wohltmann, I., von der Gathen, P., Lehmann, R., Maturilli, M., Deckelmann, H., Manney, G. L., ... Rex, M. (2020). Near-complete local reduction of arctic stratospheric ozone by severe chemical loss in spring 2020. *Geophys. Res. Lett.*, *47*(20), e2020GL089547. doi: 10.1029/2020GL089547

Zoogman, P., Liu, X., Suleiman, R. M., Pennington, W. F., Flittner, D. E., Al-Saadi, J. A., ... Chance, K. (2017). Tropospheric emissions: Monitoring of pollution (TEMPO). *Journal of Quantitative Spectroscopy and Radiative Transfer*, *186*, 17-39. (Satellite Remote Sensing and Spectroscopy: Joint ACE-Odin Meeting, October 2015) doi: 10.1016/j.jqsrt.2016.05.008

Supporting Information for "NASA GEOS Composition Forecast (GEOS-CF) system version 1: Evaluation of the stratospheric composition against independent observations"

K. E. Knowland[1,2], C. A. Keller[1,2], P. A. Wales[1,2], K. Wargan[2,3], L. Coy[2,3], M. S. Johnson[5], J. Liu[1,4], R. A. Lucchesi[2,3], S. D. Eastham[6,7], E. Fleming[3,4], Q. Liang[4], T. Leblanc[8], N. J. Livesey[9], K. A. Walker[10], L. E. Ott[2], S. Pawson[2]

[1]Universities Space Research Association (USRA)/GESTAR, Columbia, MD, USA

[2]NASA Goddard Space Flight Center (GSFC), Global Modeling and Assimilation Office (GMAO), Greenbelt, MD, USA

[3]Science Systems and Applications (SSAI), Inc., Lanham, MD, USA

[4]Atmospheric Chemistry and Dynamics Laboratory, NASA GSFC, Greenbelt, MD, USA

[5]Earth Science Division, NASA Ames Research Center, Moffett Field, CA, USA

[6]Laboratory for Aviation and the Environment, Department of Aeronautics and Astronautics, Massachusetts Institute of Technology, Cambridge, MA, USA

[7]Joint Program on the Science and Policy of Global Change, Massachusetts Institute of Technology, Cambridge, MA, USA

[8]Jet Propulsion Laboratory, California Institute of Technology, Wrightwood, CA, USA

[9]Jet Propulsion Laboratory, California Institute of Technology, Pasadena, CA, USA

[10]University of Toronto, Department of Physics, Toronto, Canada

Contents of this file

1. Supplementary Figures S1 to S5

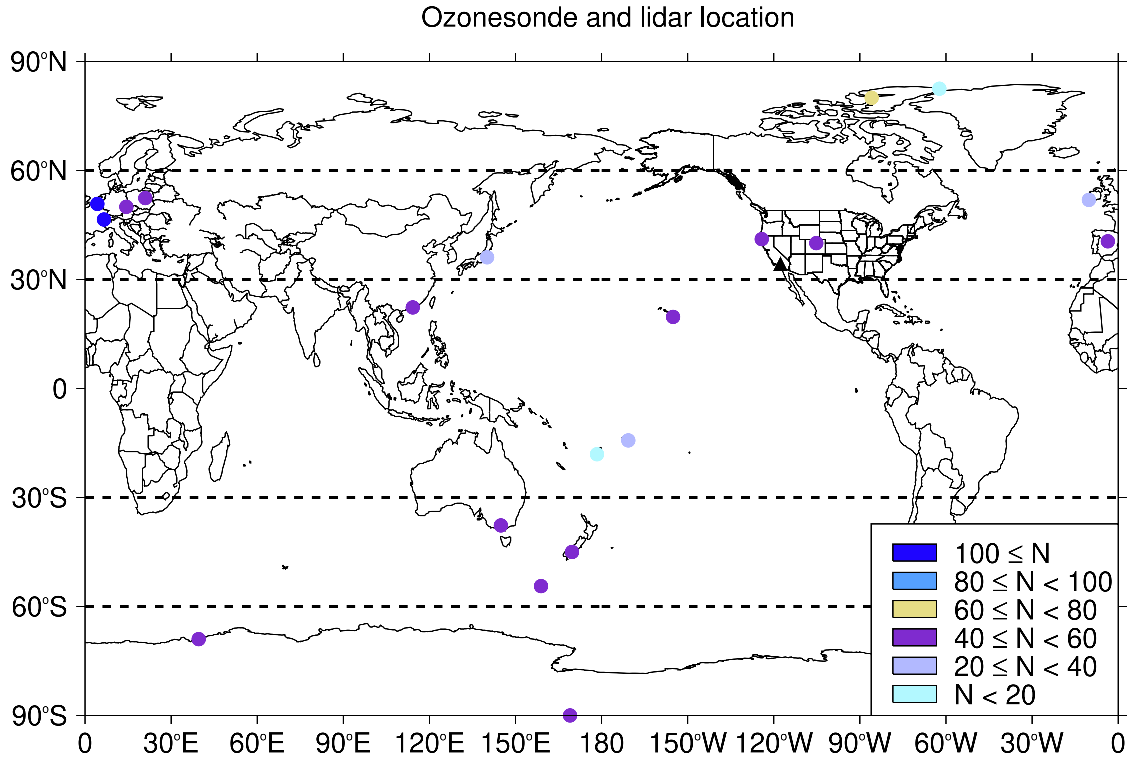

Figure S1. Ozonesonde locations colored by the number of launches in 2020 used in this study (see Table 2). Location of the NASA JPL Table Mountain Facility tropospheric O_3 lidar (TMTOL; 34.38 °N, 117.68 °W) is indicated as black triangle.

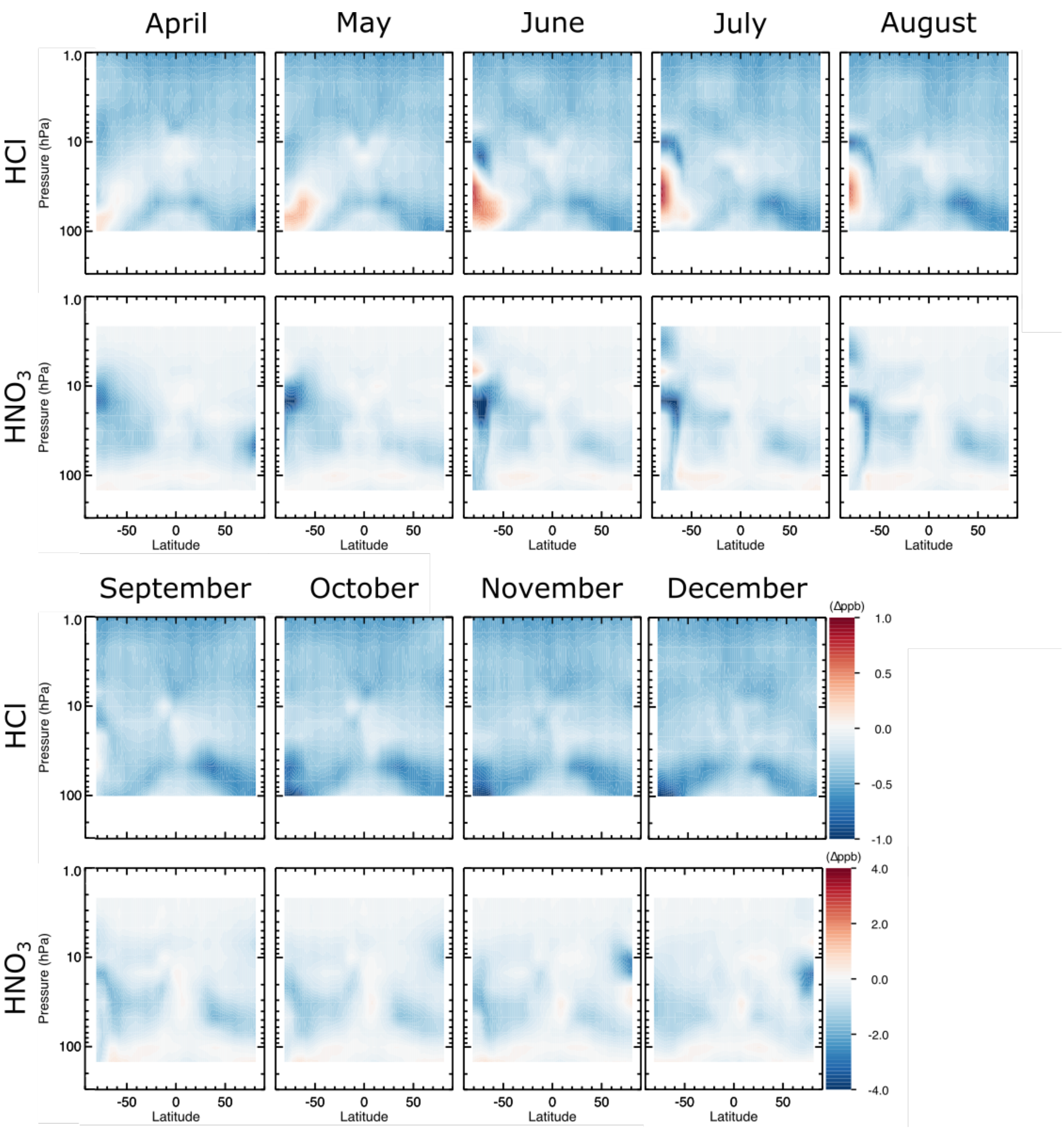

Figure S2. Zonal differences of monthly mean distributions for GEOS-CF minus MLS for HCl and HNO_3 for April to December 2020.

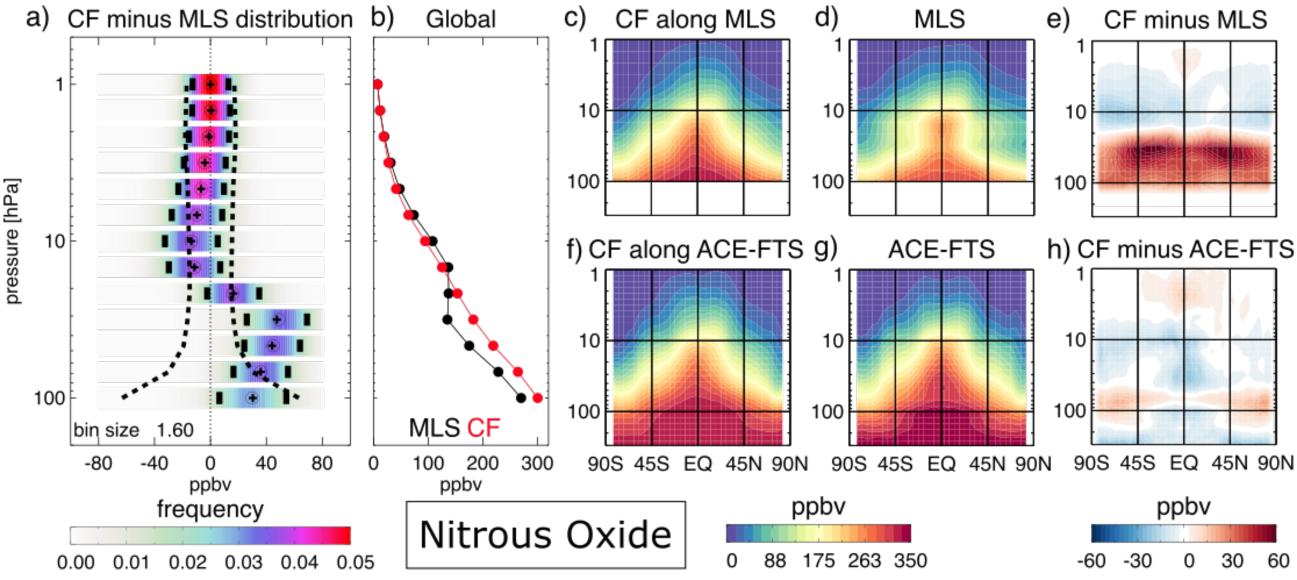

Figure S3. Similar to Figure 7 but for N_2O.

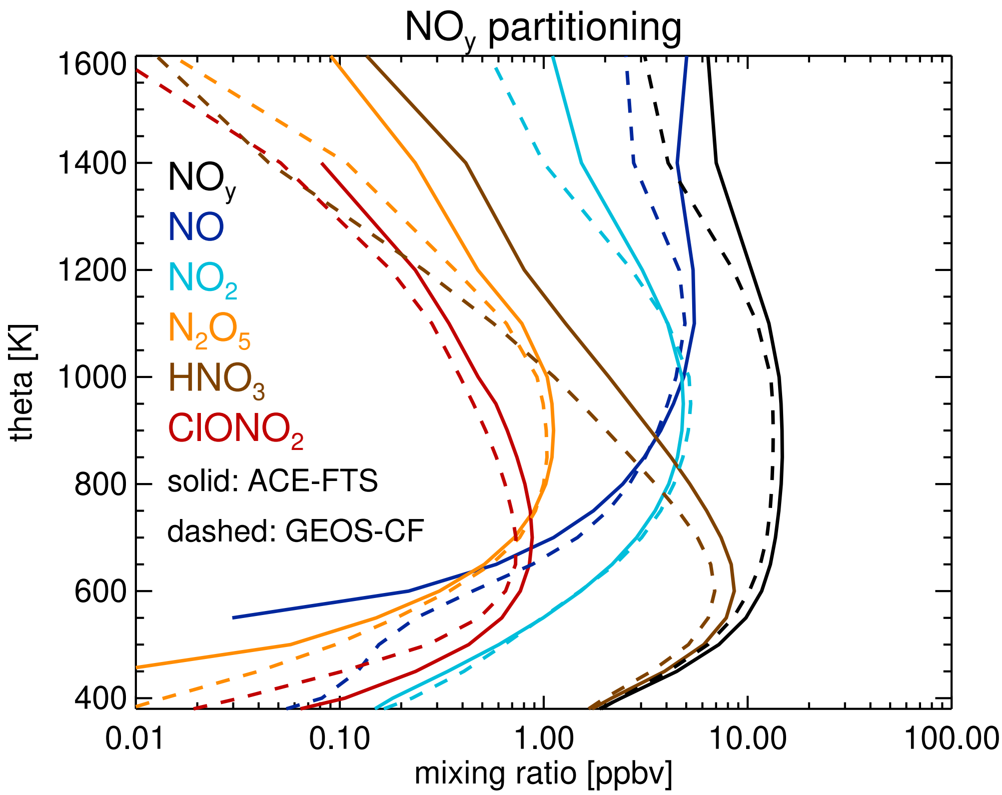

Figure S4. Cosine-weighted averages of NO_y and its components observed by ACE-FTS – NO (dark blue), NO_2 (cyan), N_2O_5 (orange), HNO_3 (brown), and $ClONO_2$ (red) – for ACE-FTS measurements (solid lines) and for matched GEOS-CF gridpoints (dashed lines).

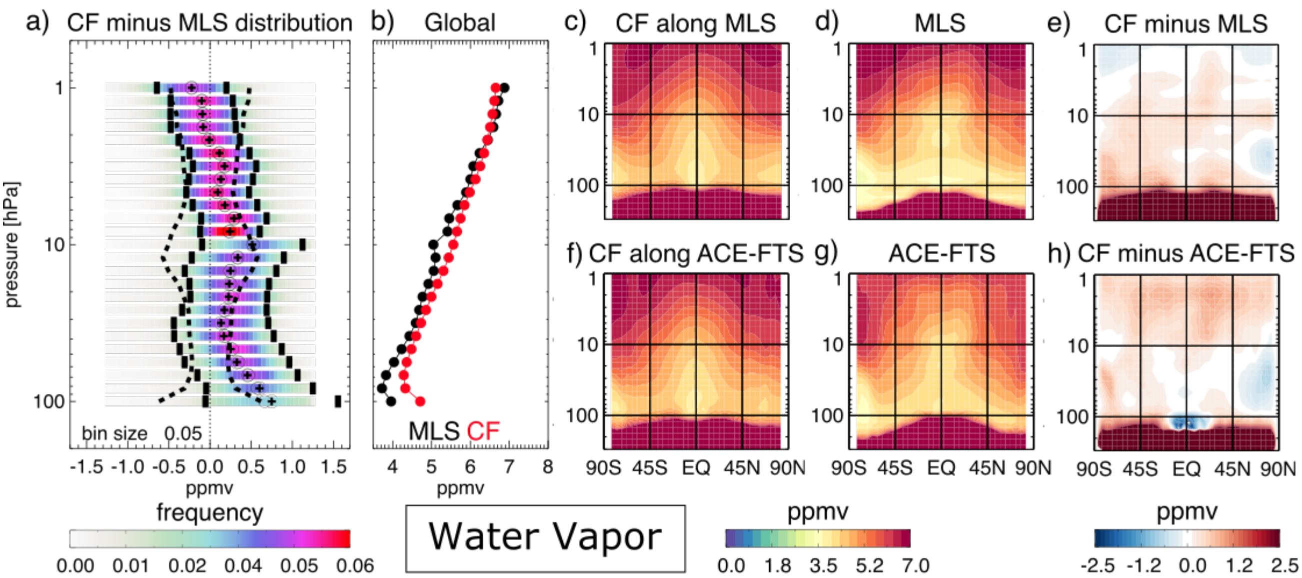

Figure S5. Similar to Figure 7 but for water vapor.